AD-A188 339 COHERENT STRUCTURE-REFLECTIVE TURBULENT VISCOUS FLOW MODELING(U) HOKENSON CO LOS ANGELES CA G J HOKENSON 07 SEP 87 HOKE-87-AF-01 AFOSR-TR-87-1660 1/1

UNCLASSIFIED F49620-85-C-0075 F/G 20/4 NL

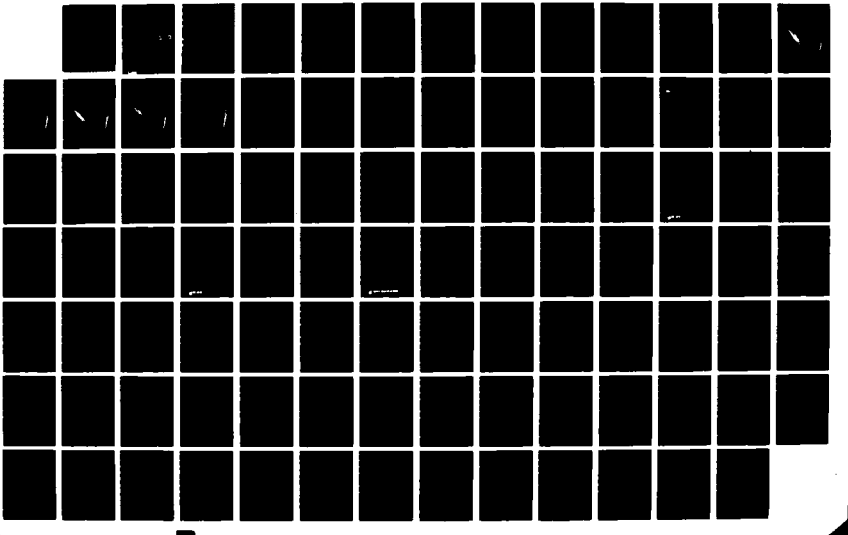

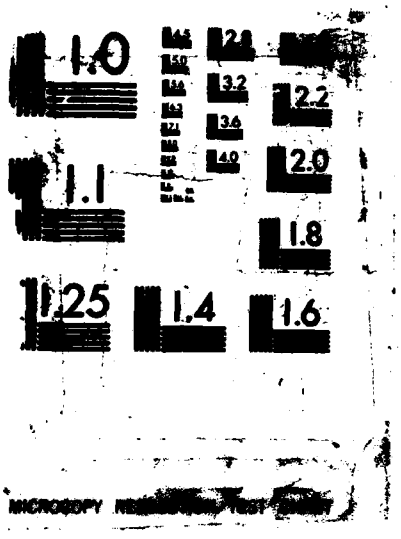
1.0
2.8
3.2
3.6
4.0
2.2
2.0
1.8
1.1
1.25
1.4
1.6
MICROCOPY

THE HOKENSON COMPANY

(2)

AFOSR-TR- 87-1660

FINAL REPORT

CONTRACT NO. F49620-85-C-0075

COHERENT STRUCTURE-REFLECTIVE TURBULENT VISCOUS FLOW MODELING

PREPARED FOR:

Dr. James M. McMichael
Program Manager
Aerospace Sciences
AFOSR/NA
Bldg. 410
Bolling AFB
Washington, D.C. 20332-6448

Original contains color plates: All DTIC reproductions will be in black and white

SEPTEMBER 1987

CHIEF EXECUTIVE • 840 S. TREMAINE AVE., LOS ANGELES, CA. 90005 • TEL. (213) 936-3743

6c ADDRESS (City, State, and ZIP Code)		7b ADDRESS (City, State, and ZIP Code)
840 S. Tremaine Ave. Los Angeles, CA 90005		Bldg 410 Bolling AFB, 20332

8a NAME OF FUNDING/SPONSORING ORGANIZATION	8b OFFICE SYMBOL (If applicable)	9 PROCUREMENT INSTRUMENT IDENTIFICATION NUMBER
AFOSR/NA	NA	F49620-85-C-0075

8c. ADDRESS (City, State, and ZIP Code)	10 SOURCE OF FUNDING NUMBERS			
	PROGRAM ELEMENT NO	PROJECT NO.	TASK NO	WORK UNIT ACCESSION NO.
Building 410 Bolling AFB, DC 20332-6448	61102F	2307	A2	

11 TITLE (Include Security Classification)

Coherent Structure Reflective Turbulent Viscous Flow Modeling (UNCLASSIFIED)

12 PERSONAL AUTHOR(S)

Dr. Gustave J. Hokenson

13a. TYPE OF REPORT	13b. TIME COVERED	14. DATE OF REPORT (Year, Month, Day)	15. PAGE COUNT
Final	FROM 3/85 TO 3/87	87-09-07	92

16. SUPPLEMENTARY NOTATION

17 COSATI CODES			18. SUBJECT TERMS (Continue on reverse if necessary and identify by block number)
FIELD	GROUP	SUB-GROUP	
1	1	16	Fluid Dynamics, Turbulence, Coherent structure

Table of Contents

Executive Summary

The research reported upon here addresses several elements of the structure of nearly parallel turbulent shear flow. Both boundary and free shear layer flows in constant as well as variable pressure fields are addressed. With respect to variable pressure conditions, unsteady as well as steady flows are embraced by the approaches. As a serendipitous consequence, many of the results also apply to flowfield separation in time-dependent flow, a topic of current interest to AFOSR. Specifically, new (and soon to be published) aspects of:

- Turbulent structure advection velocities,
- Turbulent boundary layer "instability", and
- Turbulent shear flow angular structure

have been exposed. Due to the inherent "try and fail" nature of basic research, the approximately one man-year effort invested so far has not concluded the study of any of these three areas, although four publications have resulted from the investigation. The work has, however, established the feasibility of further inquiry benefiting:

- Basic turbulence physics,
- LES and turbulence modeling, and
- Flowfield separation physics in steady and unsteady flow.

In particular, a coordinated experimental and computational study of those turbulent shear flow details which have been exposed would, in fact, serve the dual goals of understanding turbulence structure as well as separation physics.

As a direct result of the work reported here, an SBIR study of turbulence in hypersonic flow was initiated for AFOSR, the fruits of which now support an advanced R&D effort at Eglin AFB.

Discussion

The focus of the research reported upon here is the structure of nearly parallel turbulent shear flows in constant and variable pressure fields. Both wall-bounded and free shear layers were studied, as appropriate, and the variable pressure results apply to unsteady as well as steady flows. In addition, many of the results bear directly upon the generalized separation problem, addressed here insofar as it is relevant to turbulent structure details. This is reminiscent of Prandtl's view that turbulence is sustained by local separations.

The work discussed here is scheduled to be submitted for publication during the next few months. In addition, various other tangential papers which have resulted from this work have been published and are included in Appendix A.

In reporting upon the achievements of this research, it is easy to present them linearly in an orderly and coherent form. In actuality, the procedures involved where chaotic and not serial but strongly linked parallel efforts that took form only after considerable stumbling and "probing for soft spots" in the mathematics. Therefore, with this admission in the forefront, the discussion begins arbitrarily with a report on work carried out relative to the propagation of large scale structures in turbulent shear flows. The only rationale for beginning with this is its simplicity and possible surprisingly large future impact.

I. Advection Velocities

The following generalized evolution equation:

$$\frac{\partial L}{\partial t} + U_c \frac{\partial L}{\partial x} = PL + G \quad , \qquad (1)$$

arises in several applications relevant to this work:

1. As an integral boundary layer thickness equation,
2. As the equation for an instability envelope in a two-time perturbation analysis,
3. As the governing equation for the flow angle, and
4. As a pdf transport equation.

The second and third source of Eq. (1) shall be revisited in connection with the next aspects of the work to be reported. No advantage has yet been taken of the congruence to the third area.

For our purposes, the (two-dimensional or spanwise-averaged three-dimensional) time-dependent equations of motion may be integrated across the flow[1] to provide Eq. (1), wherein the following definitions apply:

$L \equiv \theta$, the momentum thickness,

$U_c \equiv U/H$, the freestream velocity divided by the shape factor,

$P \equiv$ generalized streamwise gradients term, and

$G \equiv C_f/2 + (v_w/U)(1 - u_w/U)$, the skin friction coefficient plus vectored wall mass transfer terms, times U_c.

Of interest, initially, was simply how fast large scale structures propagate. Clearly, from Eq. (1), a characteristic speed equal to H^{-1} times the local freestream velocity appears. For constant pressure turbulent boundary layers, $H \approx 1.4$ and, therefore, $H^{-1} \approx 0.7$, consistent with experimental evidence regarding certain of the largest scale structures. For our purposes, therefore, H is now <u>defined</u> by the expression:

$$\boxed{H \equiv U/U_c} \quad , \qquad (2)$$

whereas, it is computed from δ^*/θ, the ratio of displacement to momentum thicknesses. With respect to interpreting the equations, their solutions and H, physically, this orientation is more useful than discussing the δ^*/θ scale ratio.

In order to solve Eq. (1) for the evolution of a specific burst-like structure in the shear flow, P must be computed, ostensibly from the terms in its defining equation. For this study, however, an inverse approach was taken in that P itself was specified parametrically. Subsequently, the definition for P was used to solve for the implied U_c and H distribution from the equation:

$$\left\{\frac{\partial}{\partial t} + U_c' \frac{\partial}{\partial x}\right\} \ell n\, H^2 + \left\{\frac{\partial}{\partial t} + U_c'' \frac{\partial}{\partial x}\right\} \ell n\, U_c = P \quad . \qquad (3)$$

Of prime importance here is the appearance of two additional characteristic speeds of propagation,

$$U_c'/U = (H + 2)/2H \quad , \quad \text{and}$$
$$U_c'' = 2U_c' \quad . \qquad (4)$$

For a constant pressure turbulent boundary layer with H = 1.4, both U_c' and U_c'' are considerably greater than the freestream velocity, consistent with experimental observations. In addition, several aspects of these functional forms for the three characteristic speeds are clarified by the following plot:

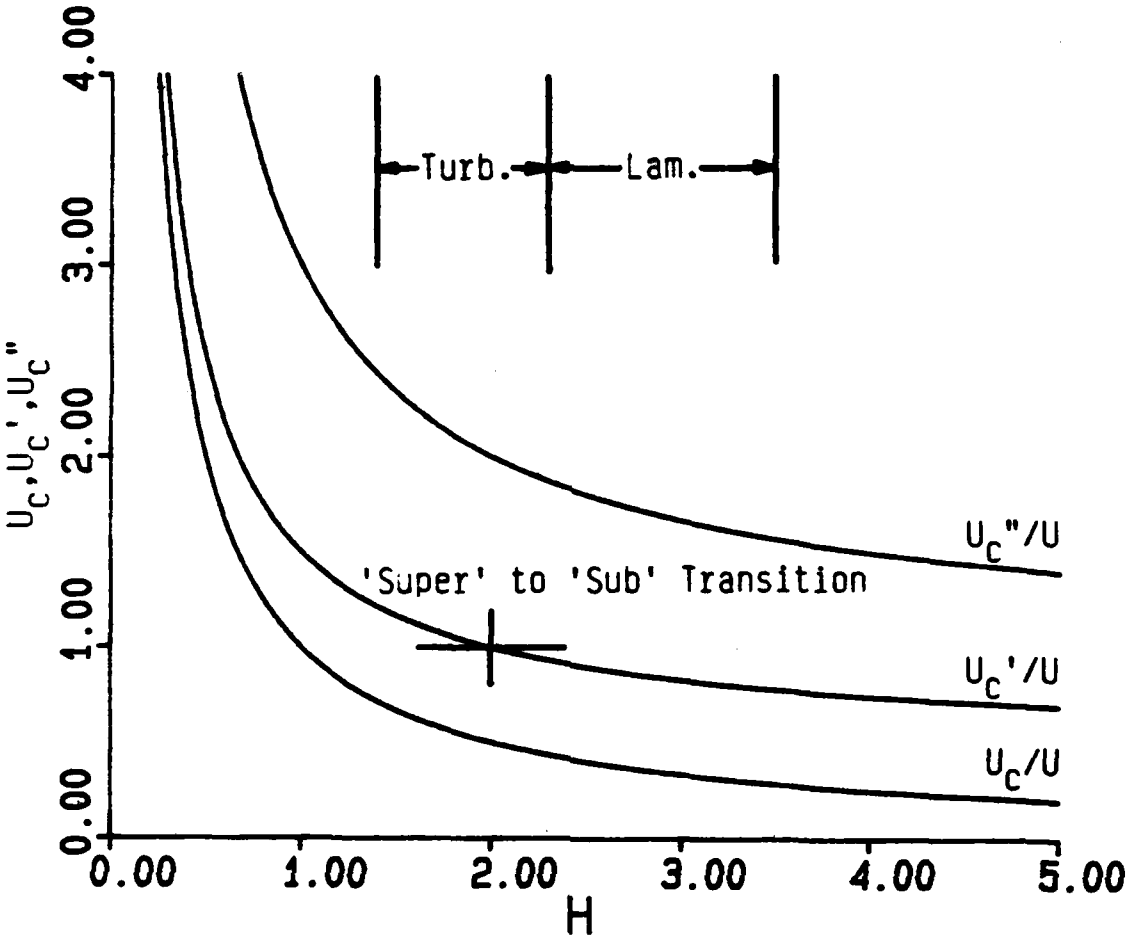

Over the range of data encountered experimentally, both U_c and U_c" are always less than and greater than freestream, respectively, for both laminar and turbulent flows. For laminar flow, U_c' is always less than freestream. However, for turbulent flow U_c' transitions from greater than freestream to less then freestream velocity at H=2. It is the hypothesis of this work, therefore, that a significant structural change in the flow relative to the propagation of large scale structures occurs at this point. Clearly, below a value of H=2.0, the freestream is not able to feed-forward information on H (carried by U_c'), as can occur above H=2.0. In addition, the broad band of experimental H values that characterize turbulent separation (~1.8 → 2.3) may merely reflect wave dynamics peculiar to the particular pressure distributions whereas the critical value of H is indeed 2.0.

With the aid of semi-empirical H and C_f laws[2], a P function which linearly ramped up in time to a Gaussian spatial distribution was input to a numerical solution of Eqs. (1) and (3). Two peak magnitudes of P were identified which forced the peak H to be in the range of 2.0 and somewhat smaller, respectively. When the flowfield solution attained equilibrium, a disturbance was injected into the flow in the form of pulsed and vectored mass transfer. For the smaller of the two peak P and, therefore, H levels, the disturbance was not catastrophic. However, at the larger peak P, the disturbance caused the shape factor to exceed 2.0 and grow exponentially, as shown in the accompanying Figs. 1&2, a-c. These results also point out the effect of this inverse approach wherein the local external flow responds to the presence of the 'bulge' in the boundary layer. This effect is critical to exposing the importance of H=2.0.

In conclusion, to the extent possible with the time and funds available, the importance of U_c' and its behavior as H changes in space and time due to steady and non-steady pressure gradients has been established.

Figs. 1 & 2, a-c.

Figs. 1: Damped Response of TBL to Pulsed Blowing. $H_{undisturbed} = 1.91$ and $v_w/U = 0.003$.

1a. Momentum Thickness

1b. Freestream Velocity

1c. Shape Factor

Figs. 2: Undamped Response of TBL to Pulsed Blowing. $H_{undisturbed} = 1.97$ and $v_w/U = 0.003$.

2a. Momentum Thickness

2b. Freestream Velocity

2c. Shape Factor

THE HOKENSON COMPANY

Figure 1a.

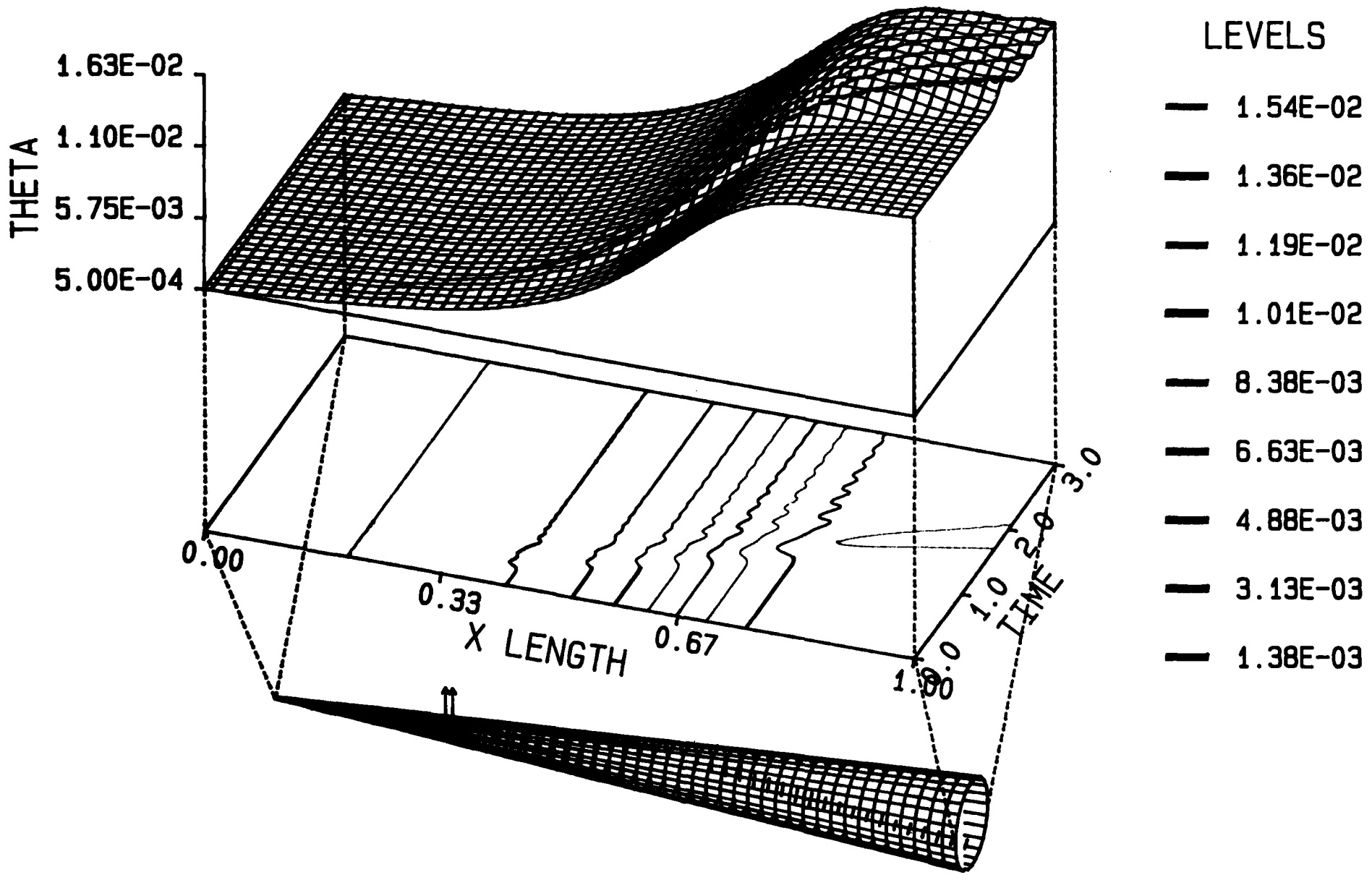

THE HOKENSON COMPANY

Figure 1b.

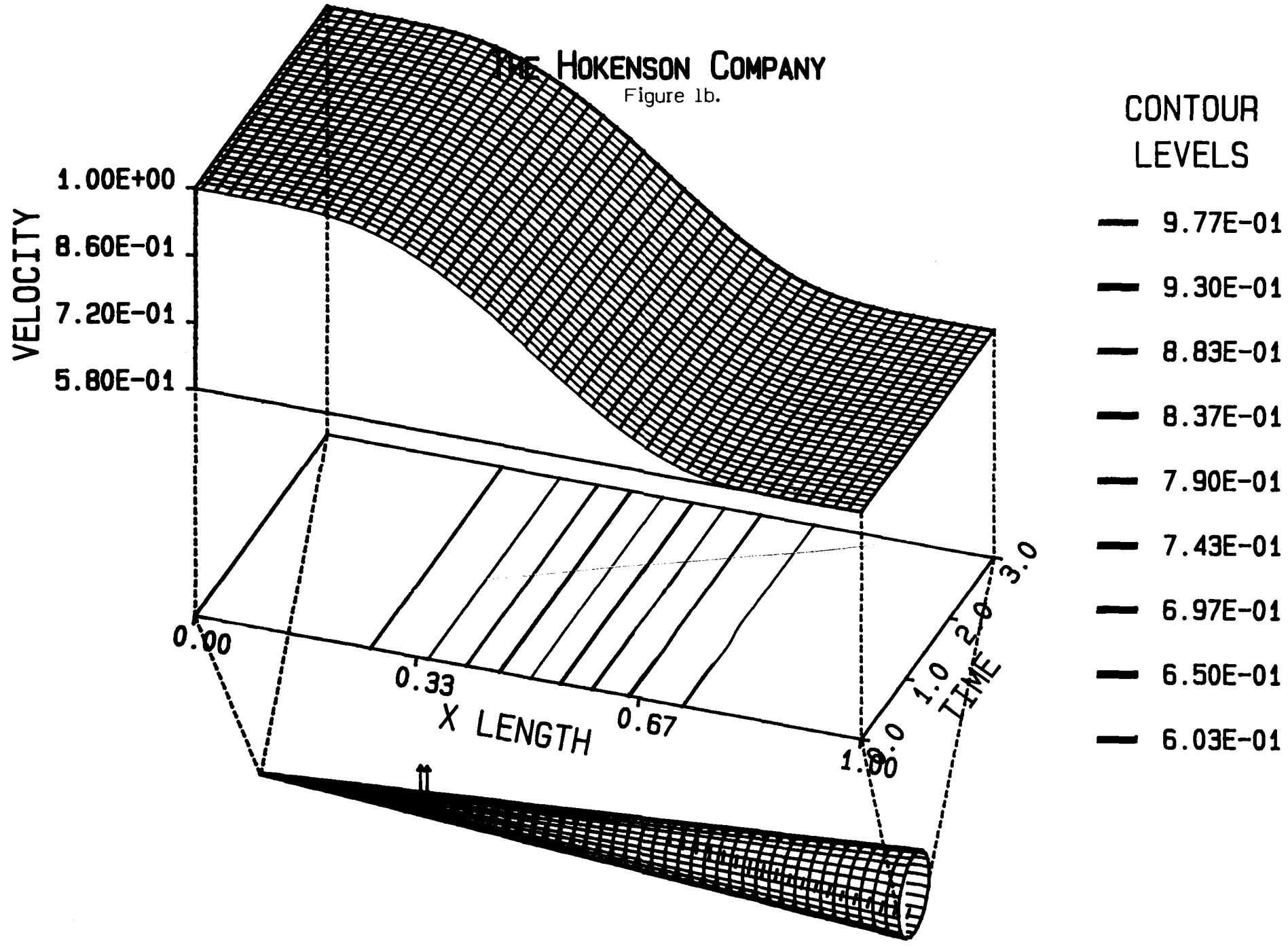

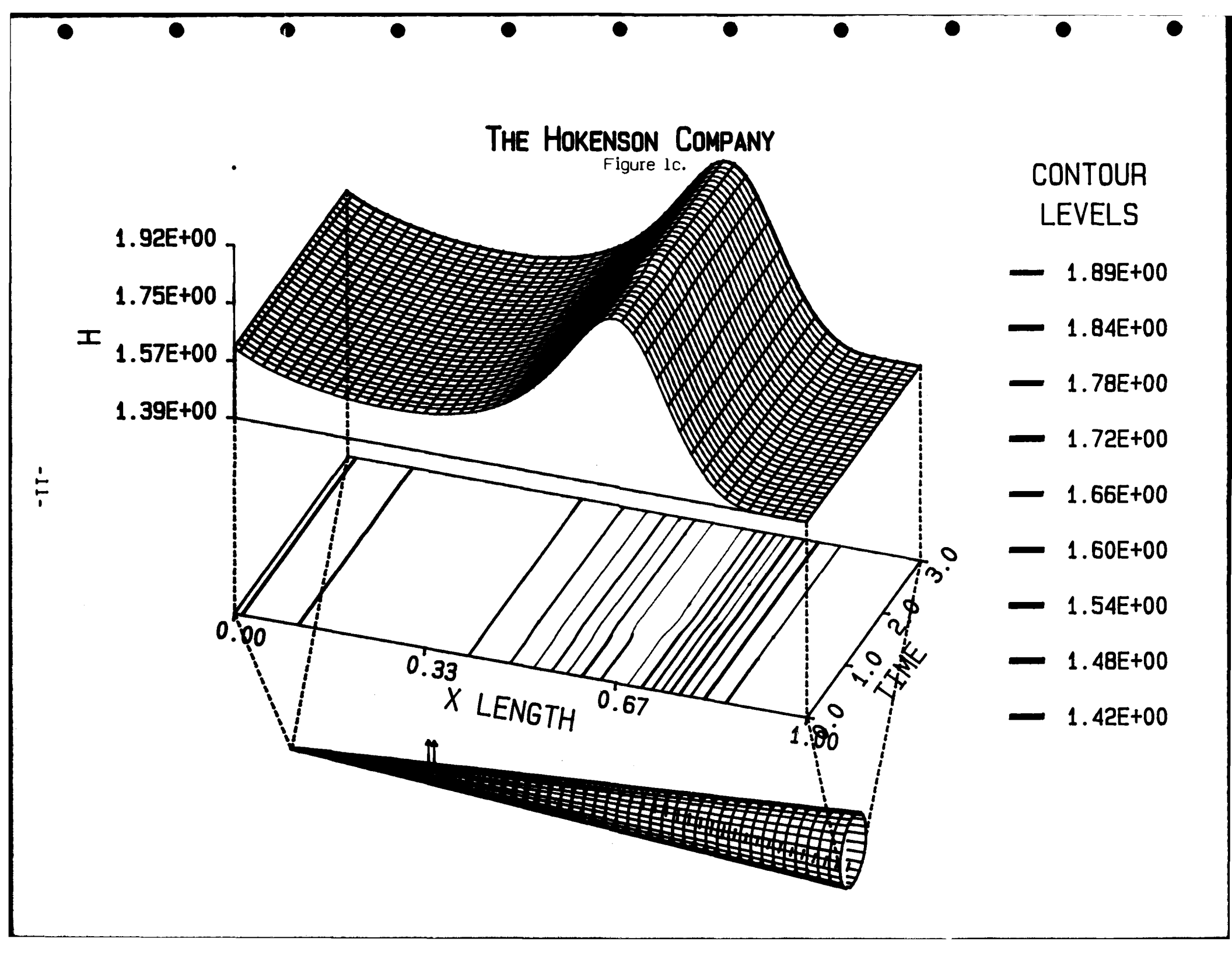
THE HOKENSON COMPANY
Figure 1c.
CONTOUR LEVELS
1.89E+00
1.84E+00
1.78E+00
1.72E+00
1.66E+00
1.60E+00
1.54E+00
1.48E+00
1.42E+00
H
1.92E+00
1.75E+00
1.57E+00
1.39E+00
0.00
0.33
0.67
1.00
X LENGTH
0.0
1.0
2.0
3.0
TIME

THE HOKENSON COMPANY

Figure 2a.

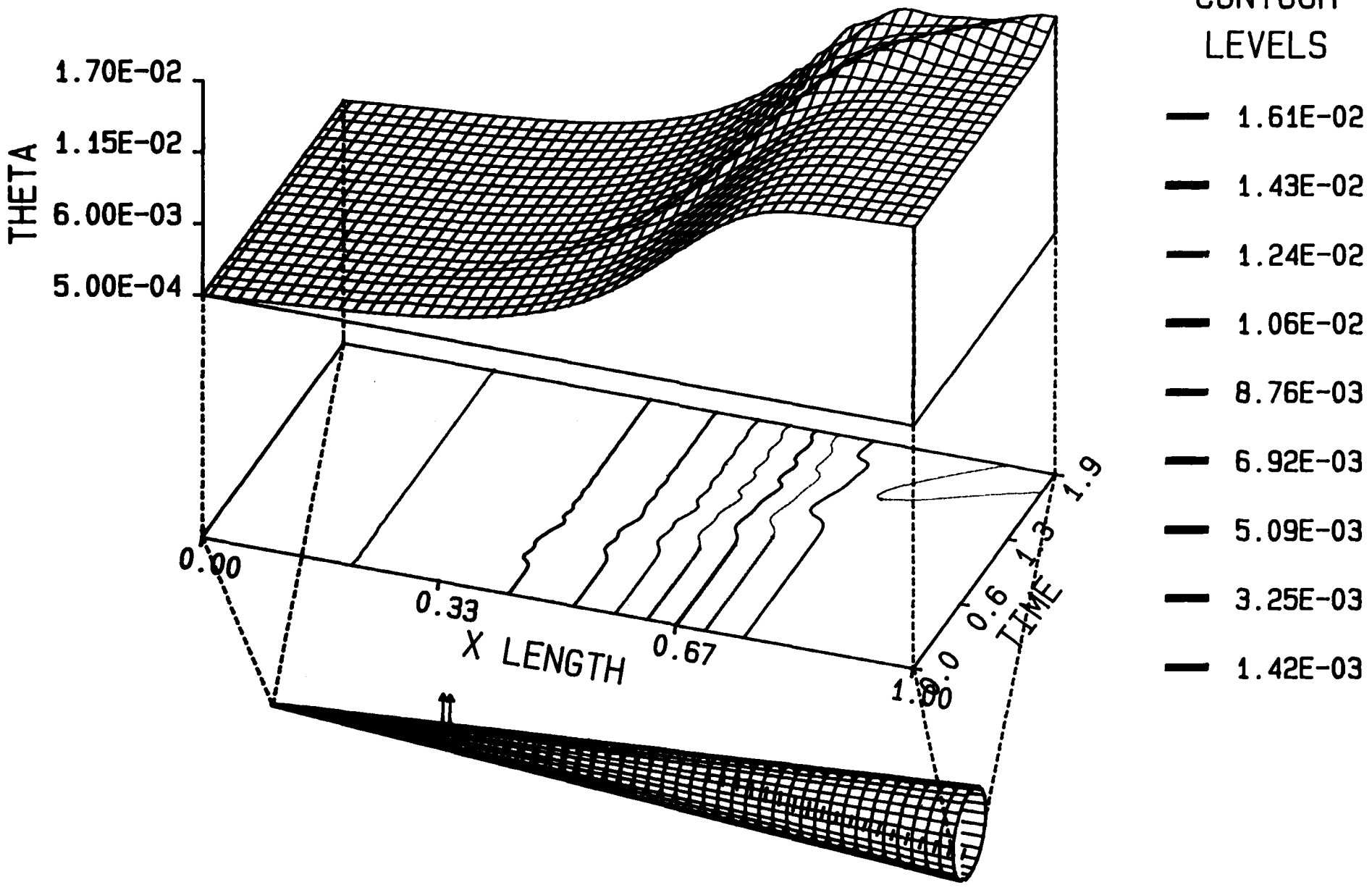

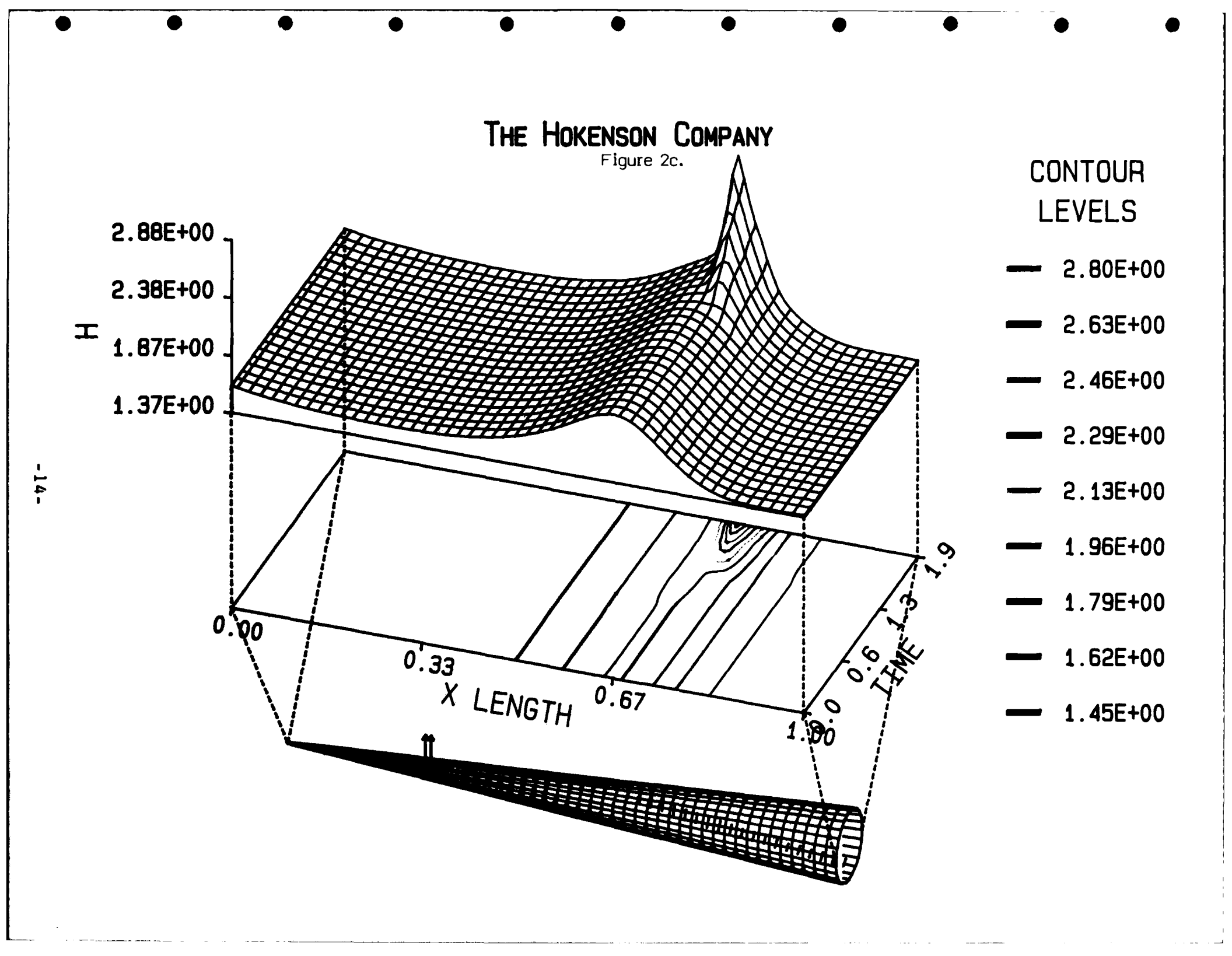
THE HOKENSON COMPANY
Figure 2c.
CONTOUR LEVELS
2.80E+00
2.63E+00
2.46E+00
2.29E+00
2.13E+00
1.96E+00
1.79E+00
1.62E+00
1.45E+00
H
2.88E+00
2.38E+00
1.87E+00
1.37E+00
0.00
0.33
0.67
1.00
X LENGTH
0.0
0.6
1.3
1.9
TIME

II. Flow Angle Structure

A. Background

Previous discussion relative to pulsed and vectored wall mass transfer indicated how this research first stumbled onto the importance of flow angles relative to vorticity transport. In particular, the vectored wall mass transfer term:

$$(1 - u_w/U)\ (v_w/U) \quad , \tag{5}$$

used to generate the pulsed disturbance discussed in the part I. of this section, was studied in the first paper included in Appendix A. Written in terms of the variables:

$$\alpha \equiv v_w/u_w \quad \text{and}$$
$$m \equiv (u_w^2 + v_w^2)^{\frac{1}{2}}/U \quad , \tag{6}$$

the vectored mass transfer term becomes:

$$\{m^2 - m(1+\alpha^2)^{\frac{1}{2}}\}\ \{-\alpha/(1+\alpha^2)\} \quad . \tag{7}$$

Equation (7) exhibits the following extrema:

$$u_w/U = 1/2, \text{ for a given } \alpha, \text{ and}$$
$$u_w/U = (1 \pm (1 + 8m^2)^{\frac{1}{2}})/4, \text{ for a given } m. \tag{8}$$

Subsequently, the research led to the second paper in Appendix A, wherein the details of vectored and pulsed mass transfer on the boundary conditions are presented. The essence of that work, as it relates to the angular structure of turbulent shear flows, may be presented in terms of the two-dimensional incompressible Navier-Stokes equations:

$$u_t + \Theta\,(u\omega) = -H_x + \nu\omega_y \qquad \text{and}$$

$$v_t - 1\,(u\omega) = -H_y - \nu\omega_x \quad , \tag{9}$$

where: $\Theta^* \equiv v/u$,

ω = vorticity and

$H \equiv p/\rho + (u^2+v^2)/2$.

Note that, evaluated at the mass transfer surface, these equations prove that the vorticity flux varies even in constant pressure flows if the mass transfer is vectored, pulsed or exhibits spatial variation.

By using the condition of flowfield incompressibility, Eqs. (9) may be cross-differentiated to provide the following expression for H:

$$\nabla^2 H = \omega^2 + u\,(\omega_y - \Theta\omega_x) \quad . \tag{10}$$

Inasmuch as streamlines (ψ) are defined by: $d\psi = udy - vdx$, along ψ = constant lines, $dy/dx = \Theta$. Therefore, the H field responds to gradients in vorticity normal to the streamlines.

*Note that Θ was also used to represent the momentum thickness in part I.

By manipulating Eqs. (9), the following expression ensues:

$$\Theta_t - \omega = -(H_y - \Theta H_x)/u - \nu(\omega_x + \Theta\omega_y)/u \quad , \qquad (11)$$

where $(1+\Theta^2)$ has been approximated by 1 in the coefficient of ω for weakly non-parallel flows.

The interpretation of Eq. (11) is that Θ_t is a measure of, but lags or leads the vorticity according to cross-streamline gradients in H and along-streamline gradients in ω.

With this motivation, the basic angular structure of turbulent shear flows is being analyzed to expose the physics and aid the modeling. As this report is being written, a fully three-dimensional solution of a nominally two-dimensional free shear layer is being completed, which forms the basis for a future investigation and publication.

B. Development

For the purposes of exposition, consider initially a two-dimensional flowfield $(u,v;x,y)$ and examine the behavior of the angular tangent variable :

$$\Theta \equiv v/u \quad . \tag{12}$$

By applying traditional Reynolds decomposition, it may be shown that:

$$\bar{\Theta} - \underline{\Theta} = - \overline{\theta' u'}/\bar{u} \quad , \tag{13}$$

where: $\underline{\Theta} \equiv \bar{v}/\bar{u}$.

In addition:

$$\overline{\theta' u'} = (\overline{u'v'} - \bar{\theta}\overline{u'^2})/\bar{u} \quad . \tag{14}$$

By combining Eqs. 13 & 14, the following expression ensues:

$$\bar{\Theta} - \underline{\Theta} = \bar{R} + \bar{\Theta}(\overline{u'^2}/\bar{u}^2) \quad , \tag{15}$$

where: $\bar{R} \equiv \overline{u'v'}/\bar{u}^2$,

herein referred to as the local Reynolds stress correlation coefficient.

For small $\bar{\theta}$ and turbulence intensity, Eq. (15) may be approximated by:

$$\boxed{\bar{\theta} - \underline{\theta} = \bar{R}} \quad , \tag{16}$$

which has the obvious interpretation that the difference between the mean flow angle and the angle of the mean flow is equal to the local Reynolds stress correlation coefficient. In addition, even on lines of symmetry when $\underline{\theta} = 0$, $\bar{\theta}$ may be non-zero and is equal to $\bar{R}$, with the aforementioned restrictions.

In order to form various correlations, neglecting higher order fluctuation products, the fluctuating angle may be written:

$$\boxed{\theta' = \underline{\theta}(v'/\bar{v}) - \bar{\theta}(u'/\bar{u}) + H.O.T.} \quad , \tag{17}$$

where: $$H.O.T. \equiv (\overline{\theta' u'} - \theta' u')/\bar{u} \quad .$$

In the four quadrant decomposition[3] of coherent structure data, the second and fourth quadrant contribute most to the net production of Reynolds stresses, associated with the ejection and sweep. Clearly from Eq. (17), θ' is largest when v' and u' are of the opposite sign, as in the second and fourth quadrant. However, v' and u' are weighted by $\underline{\theta}$ and $\bar{\theta}$, which differ by $\bar{R}$. Therefore, the behavior of $\bar{\theta}$ and θ' is significant and, in conjunction with conventional approaches to obtain $\bar{v}$ and $\bar{u}$, and thus $\underline{\theta}$, may be a more effective way of exposing, e.g., the Reynolds stress structure.

C. Analysis

As shown in Appendix B, the full N-S equations may be written in terms of angular variables in the form:

$$N_{3t}\,\Theta = (G - \Theta F)/u \quad \text{and}$$

$$N_{3t}\,\alpha = (H - \alpha F)/u \quad , \tag{18}$$

where:

$$N_{3t} \equiv \partial/\partial t + u\,(\partial/\partial x + \Theta\partial/\partial y + \partial/\partial z) \quad ,$$

$$\Theta,\alpha \equiv v/u,\ w/u \quad ,$$

$$F,G,H \equiv -P_{x_i} + \nu\nabla^2 u_i \ ;\ i = 1,2,3 \quad , \quad \text{and}$$

$$P \equiv p/\rho.$$

Consider, for simplicity, an essentially inviscid, two-dimensional flow such that Eq. (18) and the continuity equation become:

$$\Theta_t + (u\Theta)_x + (u\Theta^2)_y = \Theta P_x/u \quad \text{and} \tag{19}$$

$$u_x + (u\Theta)_y = 0 \quad .$$

Written in streamfunction (x, ψ) variables, Eq. (19) becomes:

$$\theta_t + u\theta_x = \theta\,(P_x - u\theta P_\psi)/u \quad . \tag{20}$$

By expanding θ in a series, the first order weakly non-parallel solution obeys the following equation:

$$\boxed{\theta_t + u\theta_x = \theta\, P_x/u + \text{H.O.T.} \quad .} \tag{21}$$

Conveniently, this is the precise form of the momentum thickness evolution equation studied in part I. of this section. We have also exposed a new parameter, P_x/u, to investigate such that the understanding of, and ability to model coherent structure is reinforced. As this report is being written, a fully three-dimensional N-S solution of a nominally two-dimensional planar mixing layer, such as that shown in Figs. 3, is being completed for fluture publication, along with a refined version of Appendix B. The fluctuation data obtained shall be used to evaluate the angular fluctuations and various correlations thereof with respect to turbulent burst/sweep physics and transport modeling.

Figs. 3. Typical Simulations of a Free Shear Layer

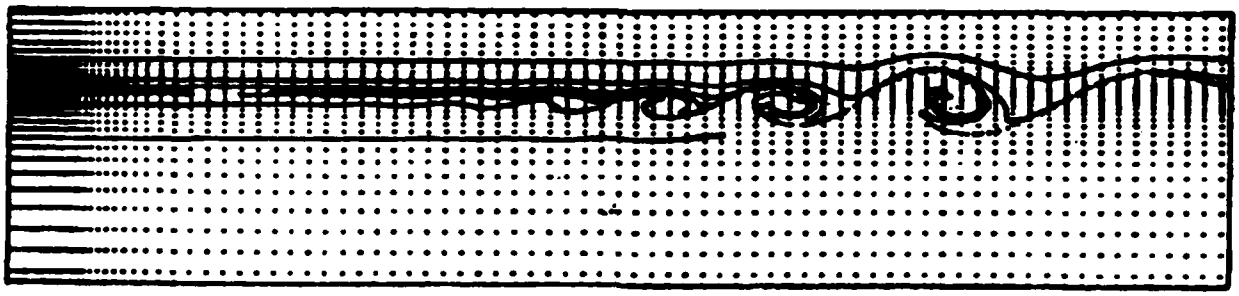

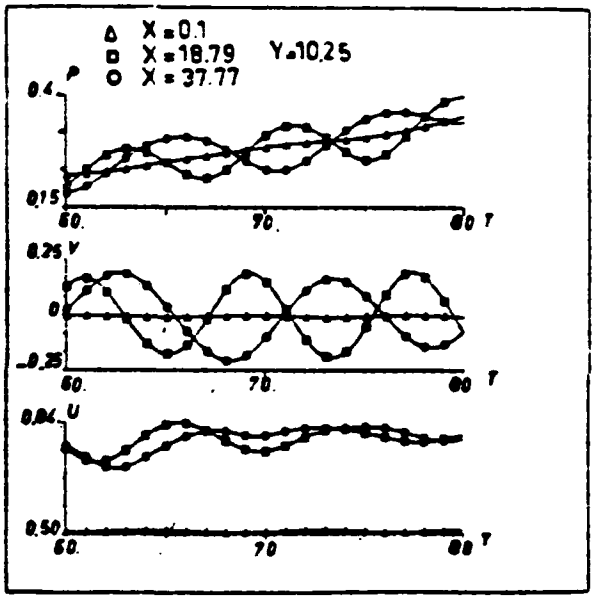

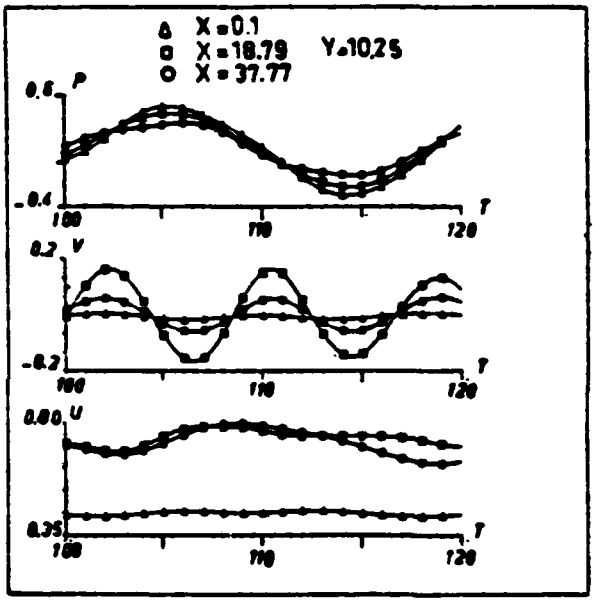

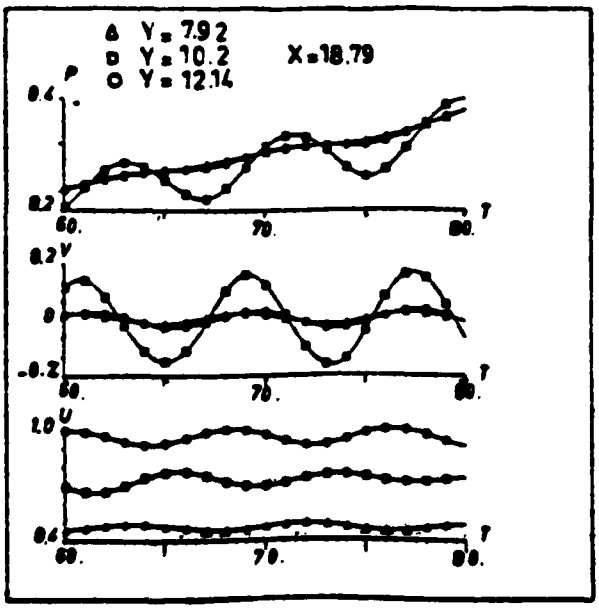

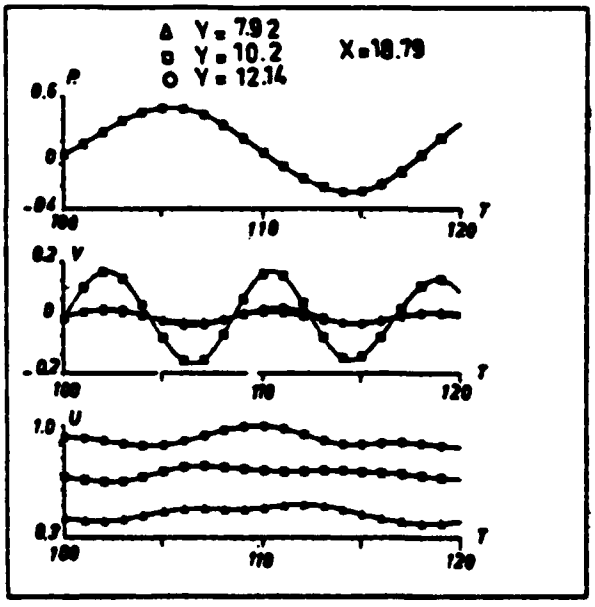

III. Instability

The pioneering work of Landahl[4] in weakly non-linear instability (wave-like) representations of turbulence forms the basis for the computations of coherent structure fluctuations which have been carried out. A multiple-element decomposition[5,6] of the governing equations was used in which temporally coherent and two distinct spatial scales of temporally incoherent fluctuations are 'superposed' in order to constitute the solution. By judicious use of appropriate time, phase and spatial averaging, governing equations for each element may be derived, as shown in Fig. 4.

Fig. 4.

A FOUR-ELEMENT DECOMPOSITION OF THE NAVIER-STOKES EQUATIONS

$$\frac{\partial U_i}{\partial t} + U_j \frac{\partial U_i}{\partial x_j} = -\frac{1}{\rho}\frac{\partial P}{\partial x_i} + \nu \frac{\partial^2 U_i}{\partial x_j \partial x_j}$$

$$\frac{\partial U_i}{\partial x_i} = 0$$

Decompose the flow into four components by:

$$\left.\begin{aligned} u_i &= U_i + \tilde{U}_i + U_i' + u_i' \\ p &= P + \tilde{P} + P' + p' \ , \end{aligned}\right\}$$

where: U_i, P = time mean flow

$\tilde{U}_i$, $\tilde{P}$ = coherent component

U_i', P' = incoherent component, large scale

u_i', p' = incoherent component, small scale

Mean Flow:

$$U_j \frac{\partial U_i}{\partial x_j} = -\frac{1}{\rho}\frac{\partial P}{\partial x_i} + \nu \frac{\partial^2 U_i}{\partial x_j \partial x_j} = \frac{\partial}{\partial x_j}\left(\overline{\tilde{U}_i \tilde{U}_j} + \overline{R}_{ij} + \overline{r}_{ij}\right)$$

$$\frac{\partial U_i}{\partial x_i} = 0$$

Coherent Flow:

$$\frac{\partial \tilde{U}_i}{\partial t} + U_j \frac{\partial \tilde{U}_i}{\partial x_j} + \tilde{U}_j \frac{\partial U_i}{\partial x_j} = -\frac{1}{\rho}\frac{\partial \tilde{P}}{\partial x_i} + \nu \frac{\partial^2 \tilde{U}_i}{\partial x_j \partial x_j} - \frac{\partial}{\partial x_j}\left(\tilde{R}_{ij} + \tilde{r}_{ij}\right)$$

$$\frac{\partial \tilde{U}_i}{\partial x_i} = 0$$

Incoherent Large Scale Flow:

$$\frac{\partial U_i'}{\partial t} + (U_j + \tilde{U}_j)\frac{\partial U_i'}{\partial x_j} + U_j' \frac{\partial}{\partial x_j}(U_i + \tilde{U}_i) = -\frac{1}{\rho}\frac{\partial P'}{\partial x_i} + \nu \frac{\partial^2 U_i'}{\partial x_j \partial x_j} - \frac{\partial}{\partial x_j}\{r_{ij}'\}$$

$$\frac{\partial U_i'}{\partial x_i} = 0$$

Incoherent Small Scale Flow

$$\frac{\partial u_i'}{\partial t} + (U_j + \tilde{U}_j + U_j')\frac{\partial u_i'}{\partial x_j} + u_j' \frac{\partial}{\partial x_j}(U_i + \tilde{U}_i + U_i') = -\frac{1}{\rho}\frac{\partial p'}{\partial x_i} + \nu \frac{\partial^2 u_i'}{\partial x_j \partial x_j}$$

$$\frac{\partial u'}{\partial x_i} = 0$$

where $\overline{}$ = time average

$\langle \quad \rangle$ = phase average

$\{ \quad \}$ = large scale average

Define fluid stresses:

$$R_{ij} \equiv \underline{U_i' U_j'} \ , \quad \text{and}$$

$$r_{ij} \equiv \underline{u_i' u_j'} \ .$$

Further, decompose these streses as:

$$R_{ij} = \overline{R_{ij}} + \tilde{R}_{ij} + \underline{R'_{ij}}$$

$$r_{ij} = \overline{r}_{ij} + \tilde{r}_{ij} + \underline{r'_{ij}} \ .$$

Of primary interest in the research reported here is the large-scale temporally incoherent fluctuating element, generally referred to as (spatially) coherent turbulent structure. The small-scale temporally incoherent element enters into and affects the coherent structure solution, however. Rather than solving the small-scale equations, the terms in the large-scale equations resulting therefrom are modeled utilizing classical gradient transport theory.[7,8,9]

The virtue of retaining temporally coherent elements in the decomposition is that unsteady flow effects on the turbulent structure may be readily incorporated.[9] In particular, the effect of various time-dependent freestream velocity fields on the turbulent transport, insofar as it affects, for example, flowfield separation, could be addressed by this formulation.

The conventional wisdom regarding the constant pressure mean turbulent flow velocity profile is that it is stable. This is clear form the work of Landahl in which fluctuation correlations arising from non-linear terms are treated as a known non-homogeneous function. The resultant Orr-Sommerfeld problem generates no unstable modes. In the present work, the temporally incoherent small-scale processes in the large-scale equations are considered to be (at least partially) functions of the large-scale solution. The modeling employed is gradient transport with a spatially-variable and non-equilibrium[10] (small-scale eddy viscosity) coefficient, ϵ. The non-equilibrium is specified to be of the form:

$$\tau_\epsilon \, D\epsilon/Dt + \epsilon = \epsilon_{eq} \quad . \tag{22}$$

The objective of this aspect of the work was to review the stability characteristics of the mean turbulent velocity profile with a spatially-variable and non-equilibrium small-scale process model and to structure the solution for spatially- and temporally-variable pressure fields. The transformed weakly non-linear vorticity equations are shown in Fig. 5. Note also the possibility of resonance between the vertical vorticity and vertical velocity.

Fig. 5.

FOURIER AND LAPLACE TRANSFORMED 3-D VORTICITY EQUATIONS

LINEARIZED LARGE SCALE MOTIONS

$$\left\{(\bar{u}-c) + \frac{1}{\alpha}\left[(Re^{-1} + \epsilon)(D^2-k^2) + (D^2\epsilon)\right]\right\}\hat{\omega}_1 = -\left\{(D\bar{u}) + \frac{1}{\alpha}(D\epsilon)(2D^2-k^2)\right\}\hat{u}_3$$

$$- \frac{\beta}{\alpha}\left\{(D\epsilon)D - (2D^2\epsilon)\right\}\hat{u}_2$$

$$\left\{(\bar{u}-c) + \frac{1}{\alpha}\left[(Re^{-1} + \epsilon)(D^2-k^2) + (D\epsilon)D\right]\right\}\hat{\omega}_2 = -\frac{\beta}{\alpha}(D\bar{u})\hat{u}_2$$

$$\left\{(\bar{u}-c) + \frac{1}{\alpha}\left[(Re^{-1} + \epsilon)(D^2-k^2) + (D^2\epsilon)\right]\right\}\hat{\omega}_3 = \left\{(D\bar{u}) + \frac{1}{\alpha}(D\epsilon)(2D^2-k^2)\right\}\hat{u}_1$$

$$+ \left\{(D\epsilon)D - (2D^2\epsilon)\right\}\hat{u}_2$$

$$+ \left\{-\frac{1}{\alpha}\left[D^2\bar{u} + (D\bar{u})D\right]\right\}\hat{u}_2$$

The mean velocity fields presented in Appendix C were taken from NBS data due to Klebanoff and a wide range of values for:

β = real span-wise wave number,

ω = real frequency,

τ_ε = non-equilibrium time constant, and

ε_{mag} = peak value of ε/ν ,

were investigated. (Note that non-dimensionalization with respect to δ^* and U is assumed throughout). The eddy viscosity distributions which were utilized are also shown in Appendix C.

As with Landahl's work, variations in the solution with β and ω were relatively un-dramatic. Therefore, at $\beta=0.1$ and $\omega=2.0$, a wide range of τ_ε values was studied. Surprisingly, the effect of non-equilibrium on the solutions was relatively minor. At a τ_ε of 1.0, various ε_{mag} values and ε spatial distributions were also studied. As long as a spatially non-uniform ε of the general form shown previously was utilized, unstable wave modes were observed. The typical results presented here in Fig. 6 indicate that, with appropriate small-scale process modeling, linear instability (indicated by $K \equiv \alpha_i/\alpha_r < 0$) of even the constant pressure mean turbulent flow velocity profile is possible. Additional results are presented in Appendix C.

THE HOKENSON COMPANY

BETA 0.100
OMEGA 2.000
EPSMAG 1.000
TAUEPS 0.000
RE NO. 44369.

Fig. 6.

SOLUTIONS OF ALPHA

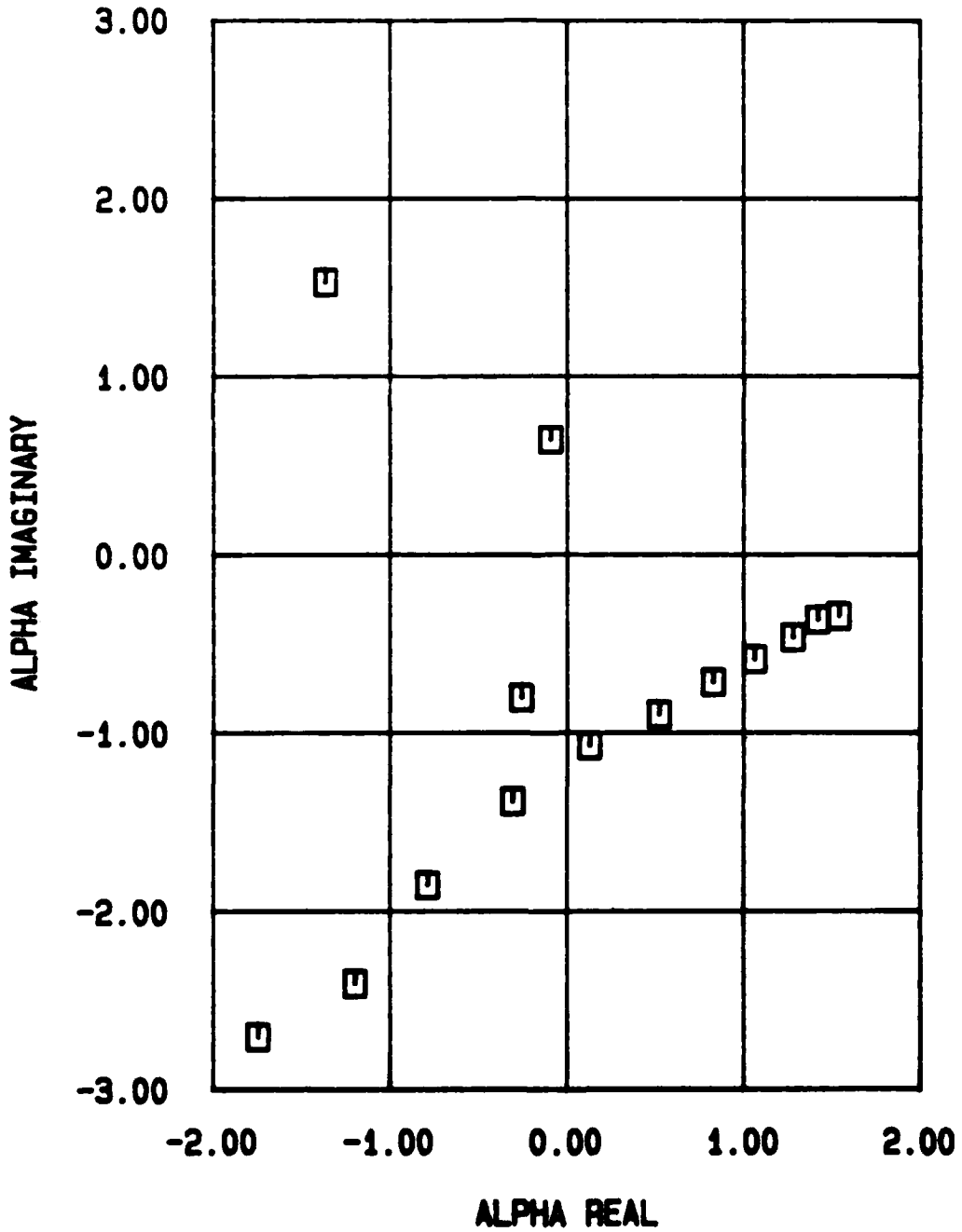

Inclusion of non-parallel effects and (spatially and/or temporally) variable freestream velocity effects are included utilizing conventional multiple-scale perturbation techniques. Note that both spatial and temporal pressure variations are represented by the temporally coherent element of the decomposition for convenience. In addition, these effects and this procedure is identical to that carried out for the evaluation of weakly non-linear terms in the large-scale structure solution itself, in the absence of temporally coherent effects. In each of these cases an amplitude evolution equation which envelopes the oscillation is derived and found to be identical in form to that of the generalized shear layer bulge evolution and angular structure equations previously studied.

Results and Conclusions

As a result of this research carried out under contract to AFOSR/NA, the following discoveries may be enumerated:

- In non-steady turbulent shear flows, one of the dominant advection velocities transitions from 'super' to 'sub', relative to the local freestream velocity, at a value of the shape factor (H) equal to 2. At this point the freestream is able to feed-forward information regarding the disturbance and catastrophic growth leading to separation occurs.
- The velocity vector angle structure of turbulent shear flows appears to be a useful variable for interpreting coherent structure data, predicting its evolution and formulating turbulent transport models.
- If adequate models of the apparent stresses in constant pressure turbulent boundary layers are employed, linearly unstable modes arise. Extension to spatially- and/or temporally-variable pressure fields is straightforward.

Based on these accomplishments, it is concluded that further work is warranted relative to:

- An experimental and detailed numerical study to corroborate the observed criticality of $H = 2$.
- Fully three-dimensional numerical simulations and experimental investigations of, for example, free shear layers in terms of their angular structure, relative to both coherent structure interpretation and modeling.
- The solution of a full initial value problem utilizing the weakly non-linear wave-guide simulations of large-scale structure.

The final result and conclusion of this effort is that it motivated an SBIR study on hypersonic turbulence for AFOSR, the fruits of which now support and advanced R&D project at Eglin AFB.

References

1. Schlichting, H., Boundary Layer Theory, McGraw-Hill, 1968, p. 393.

2. Kutateladze, S.S. and Leont'ev, A.I., Turbulent Boundary Layers in Compressible Gases, Academic Press, 1946, Chapter 5.

3. Lu, S.-S. and Willmarth, W.W., "The Structure of the Reynolds Stress In a Turbulent Boundary Layer," Univ. of Michigan Report 021490-2-T, October 1972.

4. Landahl, M.T., "A Wave-Guide Model for Turbulent Shear Flow," JFM, Vol. 29, Part 3, pp. 441-459, 1967. Also, Opening General Lecture, Recent Developments in Turbulence Research, Meeting Unknown.

5. Mollo-Christensen, E., "Physics of Turbulent Flow," AIAA J., Vol. 9, No. 7, July 1971.

6. Hussain, A. and Reynolds, W.C., "The Mechanics of an Organized Wave in Turbulent Shear Flow," JFM; Part 1, Vol. 41, 1970; Part 2, Vol. 54, 1972; Part 3, Vol. 54, 1972.

7. Liu, J.T.C., "Developing Large-Scale Wavelike Eddies and the Near Jet Noise Field," JFM, Vol. 62, Part 3, 1974.

8. Tam, C.K.W. and Chen, K.C., "A Statistical Model of Turbulence in Two-Dimensional Mixing Layers," JFM, Vol. 92, Part 2, 1979.

9. Davis, R.E., "Perturbed Turbulent Flow, Eddy Viscosity and the Generation of Turbulent Stresses," JFM, Vol. 63, Part 4, 1974.

10. Crow, S.C., "Viscoelastic Properties of Fine-Grained Incompressible Turbulence," JFM, Vol. 33, Part 1, 1968.

11. Kim, H.T., Kline, S.J. and Reynolds, W.C., "The Production of Turbulence Near a Smooth Wall in a Turbulent Boundary Leyer," JFM, Vol. 50, Part 1, 1971.

Appendix A

PUBLICATIONS

Turbulent Boundary Layers with Vectored Mass Transfer

G. J. Hokenson

Reprinted from AIAA Journal Volume 24, Number 3, March 1986, Page 528

AMERICAN INSTITUTE OF AERONAUTICS AND ASTRONAUTICS • 1633 BROADWAY • NEW YORK, N.Y. 10019

Turbulent Boundary Layers with Vectored Mass Transfer

Gustave J. Hokenson*
The Hokenson Company, Los Angeles, California

THE excellent data presented in Ref. 1 provide substantial guidance in the understanding of many of the subtleties of turbulent boundary-layer (TBL) flows with blowing, and the modeling thereof. In an effort to peel away quantitatively the various interacting elements of the flow, it is proposed that the following approach may be useful for exploiting such data in model development. If the Reynolds-averaged equations of motion are further locally spatially averaged in horizontal planes, with a scale large relative to the porosity yet small relative to the boundary-layer growth, the discrete jet blowing may be converted into its distributed mass transfer equivalent. For example,

$$\tilde{u} = \langle \tilde{u} \rangle + \tilde{u}^{\circ} \tag{1}$$

where $\tilde{u}$ is the time-averaged streamwise velocity and $\langle\ \rangle$, $(\ )^{\circ}$ denote the local spatial average and the variation therefrom, respectively. As a result of this local spatial averaging, the governing equation nonlinearities generate extra (Reynolds stress-like) terms due to the spatial variations. (Note that a piecewise constant filter function is used such that no Leonard terms appear.) In addition, the average normal velocity at the surface is now simply related to the total flow rate and area, which reduces the local jet-like values of wall normal velocity by the open area ratio of the surface, while the average skin friction is the weighted sum of the solid surface plus open surface contributions. Finally, the doubly averaged streamwise velocity and turbulence at the wall are now nonzero.

It appears that the location in the boundary layer at which $\langle \tilde{v}^{\circ} \tilde{v}^{\circ} \rangle = 0$ (where $\tilde{v}$ is the time-averaged normal velocity) defines a level that divides the relatively weakly sheared

Received June 3, 1985.
*Chief Scientist. Member AIAA.

outer flow, which is readily characterizable from even linear theory,[2] from an inner flow where the $\langle \tilde{u}^* \tilde{v}^* \rangle$ decay results from the discrete jet mixing and streamwise deflection. Given some relationship between $\langle \tilde{u} \rangle_w$, $\langle \tilde{u}^* \tilde{v}^* \rangle_w$, $\langle \overline{u'v'} \rangle_w$, and the wall structure (where $'$ denotes turbulent fluctuations and w wall conditions), the inner layer typified by high shear, relatively low speed flow may also be characterizable.[3]

In a constant pressure integral formulation (which may be most convenient for data analysis), the aforementioned phenomena may be expressed:

$$\frac{d\theta}{dx} = \left(1 - \frac{\langle \tilde{u} \rangle_w}{u_e}\right) \frac{\langle \tilde{v} \rangle_w}{u_e} - \frac{\langle \tilde{u}^* \tilde{v}^* \rangle_w}{u_e^2} - \frac{\langle \overline{u'v'} \rangle_w}{u_e^2} + \frac{C_f}{2} \quad (2)$$

where θ is the momentum thickness, C_f the skin friction coefficient, u_e the freestream velocity, and the additional terms correspond to the three effects discussed here, $\langle \tilde{u}^2 \rangle_{,x}$ having been deleted. The modeling problem that the data in Ref. 1 should significantly impact is twofold:

1) $\langle \tilde{u} \rangle_w$, $\langle \tilde{u}^* \tilde{v}^* \rangle_w$, and $\langle \overline{u'v'} \rangle_w$ all depend on the details of the flow through the particular wall. Although $\langle \tilde{u} \rangle_w$ and $\langle \overline{u'v'} \rangle_w$ may be estimated from the data, $\langle \tilde{u}^* \tilde{v}^* \rangle_w$ must be treated parametrically until a compatible solution is obtained.

2) As in all TBL modeling, C_f depends explicitly on all other effects on the right-hand side of the equation.

Therefore, some effort is required to assess which effects are important and their quantitative contribution in a general case.

Due to the relatively low blowing rates used in Ref. 1 (relative to that which would cause separation), both the vectoring effect $\langle \tilde{u} \rangle_w$ and the explicit dependence of C_f on the mass transfer may be ignored in this particular case. The resulting error of a few percent is well within the precision of the data. This allows us to focus on the representation of the terms

$$-\langle \tilde{u}^* \tilde{v}^* \rangle_w / u_e^2 - \langle \overline{u'v'} \rangle_w / u_e^2 \quad (3)$$

which are herein combined into the following single modeling expression

$$C_1 + C_2 b^2 \quad (4)$$

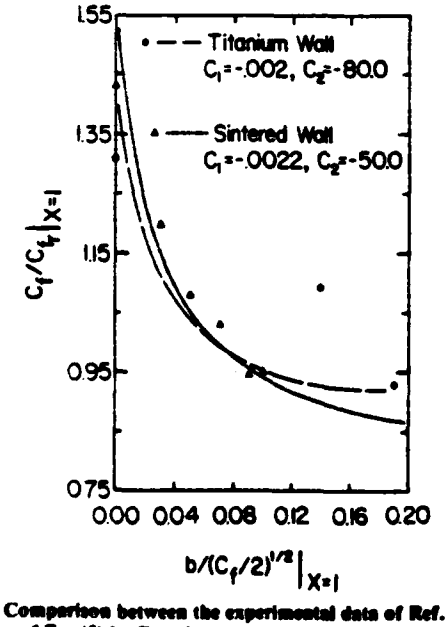

Fig. 1 Comparison between the experimental data of Ref. 1 and the modeling of Eq. (3) by Eq. (4).

where

$$b \equiv \langle \tilde{v} \rangle_w / u_e \quad (5)$$

By systematically varying the constants C_1 and C_2, the data may be fit reasonably well with $C_1 = 0.002$ and $C_2 = -80.0$ for the titanium wall, whereas $C_1 = -0.0022$ and $C_2 = -50.0$ are indicated for the sintered wall, as shown in Fig. 1. Clearly, C_1 scales with C_f and C_2 scales with C_f^{-2}, implying that the friction velocity is the appropriate reference. Note that, since the coefficients are negative, it is evident that the effect of $-\langle \tilde{u}^* \tilde{v}^* \rangle_w$ is dominant since we expect $-\langle \overline{u'v'} \rangle_w$ to be positive.

If this functional dependence persists, analysis suggests that a rise in the measured C_f is possible, over a range of larger b values than used in Ref. 1, prior to a falloff at still higher mass transfer rates. It also should be mentioned that, in measurements of forces on such a porous plate, the drag would reflect only the solid surface portion of the C_f in this form of the boundary-layer equations. However, the measured force would include a pressure difference within the passages of the porous wall due to the $\tilde{m}\langle \tilde{u} \rangle_w$ vectoring (seen in the boundary-layer equation), which also involves the contribution to C_f averaging from the open surface.

For cases in which the induced mass transfer vectoring, and $\langle \tilde{u} \rangle_w$, is significant, angle (α)/magnitude (m) variables may be appropriate. Utilizing the following definitions of α, m:

$$\alpha \equiv \langle \tilde{v} \rangle_w / \langle \tilde{u} \rangle_w \quad (6)$$

$$m \equiv (1 + \alpha^2)^{\frac{1}{2}} \langle u \rangle_w / u_e \quad (7)$$

the vectored blowing term in the boundary-layer equation becomes

$$[m^2 - m(1 + \alpha^2)^{\frac{1}{2}}][-\alpha/(1 + \alpha^2)] \quad (8)$$

The magnitude m responds to the pressure difference across the porous surface and its "loss coefficient," whereas α provides a sensitive measure of the induced vectoring, which also depends on the flow within the porous wall through $\langle \tilde{u}^* \tilde{v}^* \rangle_w$ and $\langle \overline{u'v'} \rangle_w$. The mass transfer term in this form exhibits extrema with which the effect of vectoring may be evaluated. For a given α, this term exhibits an extremum when $\langle \tilde{u} \rangle_w / u_e = \frac{1}{2}$ and, for a given m, when $\langle \tilde{u} \rangle_w / u_e = (1 \pm (1 + 8m^2)^{\frac{1}{2}})/4 \simeq -m^2, \frac{1}{2} + m^2$. Since $\langle \tilde{u} \rangle_w$ will be >0 yet $\ll \frac{1}{2}$, the effect of naturally induced vectoring could be relatively small. The effect of actively imposed optimal mass transfer vectoring is currently being studied for both steady and unsteady flows and will be the subject of a future paper.

Acknowledgment

This work was carried out under the sponsorship of the Aerospace Sciences Directorate, AFOSR and the Office of Basic Energy Sciences, Department of Energy.

References

[1]Collier, F. S. Jr. and Schetz, J. A., "Injection into a Turbulent Boundary Layer Through Different Porous Surfaces," *AIAA Journal*, Vol. 22, June 1984, pp. 839-891.

[2]Hokenson, G. J., "Linearized k-ϵ Analysis of Free Turbulent Mixing in Streamwise Pressure Gradients with Experimental Verification," *Journal of Applied Mechanics*, Vol. 46, No. 3, Sept. 1979, pp. 493-498.

[3]Hokenson, G. J., "Boundary Conditions for Flow Over Permeable Surfaces," *Journal of Fluids Engineering*, Vol. 107, No. 3, Sept. 1985, pp. 430-432.

Reprinted from September 1985, Vol. 107, Journal of Fluids Engineering

Boundary Conditions for Flow Over Permeable Surfaces

G. J. Hokenson[1]

Introduction

The subject of this work is viscous flow adjacent to a permeable surface and the boundary conditions appropriate thereto [1]. Our objective is to generalize and extend the analysis in references [2 and 3] from first principles in order to clarify the relationship between the experimental reality of a distribution of discrete nonuniform jets in a crossflow and computations which employ continuous (locally uniform) normal velocity and zero slip boundary conditions. The hypothesis is that some details of the (vortical) flow passing through the boundary and the external (partially slipping [1]) flow along the boundary affect the qualitative structure of the solution.

The analysis presented here is an extension of the work described in reference [4] and is directed at continuum flow phenomena. Although, for most problems of practical importance, we are generally interested in turbulent flow, a laminar flow is considered here to expose the particulars of the premise. Some of the results, therefore, bear directly on current interest in laminar flow control by suction. The role which turbulent flow considerations play shall be discussed subsequently. Finally, the restriction that a boundary layer structure be maintained, forcing limitations on the mass transfer magnitude, shall not be invoked.

Background

Consider first the detailed picture of a porous wall as a distribution of discrete jets. (The case of blowing will be used for purposes of discussion.) By placing a "jump-type" control volume at the exit plane of an individual jet, the results of reference [4] indicate that the external flow "slips" over the jet (i.e., the mass transfer vector tilts) with a velocity determined by:

$$\delta(\rho u v) = \delta\tau, \tag{1}$$

where δ signifies the jump in values of the variables across the control volume. Conventional notation assigns ρ, u, v, and τ to the fluid density, streamwise velocity, normal velocity and shear stress, respectively. Invoking continuity:

$$\delta(\rho v) = 0, \tag{2}$$

[1]Chief Scientist, The Hokenson Company, Los Angeles, Calif., Mem. ASME.

Contributed by the Fluids Engineering Division of The American Society of Mechanical Engineers. Manuscript received by the Fluids Engineering Division, February 4, 1984.

across the control volume allows us to write equation (1) as:

$$\delta u = \delta\tau/\rho v. \tag{3}$$

This result shall now be generalized to an arbitrarily permeable surface for comparison to the aforementioned zero slip, (locally) constant normal velocity boundary condition theoretical formulation. For cases in which u and τ within the boundary are zero, equation (3) is compatible with the results in [1-3].

Development

Consider the flow along a porous surface composed of a distribution of openings which is specified statistically in terms of size and location. The external flow is assumed to be two-dimensional, however, extension of the results to include three-dimensional effects is straightforward and will be noted. A local averaging process is now invoked [3] in planes parallel to the boundary.[2] The spatial scales of the averaging are large relative to the porosity yet small relative to the streamwise (and span-wise) variations in the mean flow. Each of the variables is decomposed into its local spatial mean plus a perturbation (e.g., $u = \langle u\rangle + u^0$). When this decomposition is applied to the Navier-Stokes equations for constant density flow, the resulting equations may be spatially-averaged to provide the result:

$$\langle u\rangle_x + \langle v\rangle_y = 0 \tag{4}$$

$$\langle u\rangle_t + (\langle u\rangle^2)_x + (\langle u\rangle\langle v\rangle)_y = -\langle p\rangle_x/\rho - \langle u^{0^2}\rangle_x - \langle u^0v^0\rangle_y + \nu\langle\omega\rangle_{(z)y} \tag{5}$$

$$\langle v\rangle_t + (\langle u\rangle\langle v\rangle)_x + (\langle v\rangle^2)_y = -\langle p\rangle_y/\rho - \langle v^{0^2}\rangle_y - \langle u^0v^0\rangle_x - \nu\langle\omega\rangle_{(z)x}, \tag{6}$$

where subscripts denote differentiation and subscripts in parentheses denote a vector component.[3] Not surprisingly, this is reminiscent of Reynolds decomposition for turbulent flow. Additional terms required for three-dimensional mean flows are apparent. If we now apply the jump-type control volume to the permeable boundary over the averaging domain, the results analogous to reference [4] are:

$$\delta\langle v\rangle = 0 \tag{7}$$

$$\langle v\rangle\delta\langle u\rangle = -\delta\langle u^0v^0\rangle + \nu\delta\langle\omega\rangle_{(z)} \tag{8}$$

$$\delta(\langle\overset{0}{v}\rangle^2) = -\delta\langle p\rangle/\rho - \delta\langle v^{02}\rangle. \tag{9}$$

In this representation, total mass flow through the permeable boundary and shear force on it are locally equivalent (over the averaging area) between the discrete and continuous representations. The average mass flux is reduced from that in the discrete jets by the ratio of open to total surface area. The average shear stress is reduced from that on the solid interstices by the ratio of solid surface area to total surface area. Some new features appear, however. Most importantly the average streamwise velocity at the boundary is nonzero and related to that in the boundary (allowing for the possibility of obliquely-oriented jets) by equation (8). The subtleties of such a situation (whether due to geometrical or flow-induced obliquity) regarding effects of internal normal stresses versus surface shear stresses and interpretation of experiment-theory comparisons with the appropriate boundary conditions is clarified by equation (8). This relationship also embodies information on the injected flow vorticity and structure.

Applying the same decomposition, averaging and jump-type boundary control volume analysis to the full equations in vorticity variables results in:

$$\langle v\rangle\delta\langle\omega\rangle_{(z)} = -\delta\langle v^0\omega^0{}_{(z)} - w^0\omega^0{}_{(y)}\rangle + \nu\delta\langle\omega\rangle_{(z)y}, \quad \text{and} \tag{10}$$

$$\delta\langle v^0\omega^0{}_{(x)}\rangle = \delta\langle u^0\omega^0{}_{(y)}\rangle, \tag{11}$$

which provides often-needed information on flow curvature at the wall.

Discussion

Therefore, we have established a relationship between the discrete distribution of jets in experiments and the continuous mass flux/shear stress distributions in computational predictions, as long as $\langle u\rangle \neq 0$ at the boundary. If $\langle u\rangle$ is set equal to zero at the boundary, calibration of some aspects of the theoretical formulation with experimental data must compensate for the approximation. It may be that the magnitude of the slip is small, inherently or due to term cancellation in equation (8). However, the structure of the injected flow does now enter the problem. Possibly, the appropriate slip velocity (guided by equation (1)) may be obtained empirically by judicious iteration between observation and theory.

However, the formulation suggests several more systematic approaches. First, since jet structures may be reasonably parameterized, the situation is much simpler than turbulence in representing the nonlinear terms. Therefore, a quantitative assessment of the effect of differences in detailed structure between porous boundaries which are equivalent in the mean is possible. Secondly, it suggests that applying computational boundary conditions at some height off the wall for which $\langle u^0v^0\rangle \simeq 0$, analogous to the flow over a wall film, may be more appropriate.

Consider these two uses of equation (8). Across the boundary, $\delta\langle u\rangle$ may be computed if we know something of the injected flow structure. It is clear that, over the openings u^0 and $v^0 > 0$ and over the solid portion u^0 and $v^0 < 0$. Therefore, $\langle u^0v^0\rangle$ is a positive number. Given $\langle v\rangle$, $\langle u\rangle$ at the wall may be computed (as a function of $\langle\omega\rangle$ at the wall, as required computationally) by specifying typical detailed distributions of u^0 and v^0 of interest within the porous boundary, computing their jump across the boundary according to equation (1) and then averaging. The procedure is necessarily iterative, requiring an initial guess of the slip velocity.

Furthermore, assuming that the height above the boundary at which $\langle u^0v^0\rangle \simeq 0$ is small, the jump expressions may be applied (to some lesser degree of accuracy) between it and the wall boundary. Note that the jump across the boundary must first be computed. In this manner the equations are used to provide the boundary conditions ($\langle v\rangle$ and $\langle u\rangle$) for computations at that level where the discrete jets have mixed out. This is reminiscent of using wall functions and, indeed, some profile hypothesis is required to do this accurately. If explicit account of the injected turbulence is of interest, the turbulence kinetic energy and length scale at the displaced height could be computed from model equations utilizing the jump-type control volume analysis. This is relevant to the comment in reference [5] in which the authors refer to blowing as "provoking the viscous sub-layer." Utilizing the approach developed here, the extent to which the injected flow structure totally disrupts the near wall conditions may be assessed.

Consider the two-equation k-ϵ model as an example only, not necessarily proposed here as a general computational tool for these flows. In this preliminary evaluation, we assume that the low Reynolds number postulates, relative to the near

[2] Note that the averaging weighting function was chosen to be a constant over the averaging domain and zero outside of it. In this manner Reynolds averaging rules are retained and the so-called Leonard terms do not appear.

[3] This formulation also significantly clarifies the effect of mass transfer on the wall vorticity flux. If $\langle u\rangle$ is nonzero (due to active vectoring or naturally with nominally normal injection), $\langle\omega\rangle_{(z)y}$ responds to the four advective terms in equation (5) even in constant pressure flows. If $\langle u\rangle$ is also nonsteady, the $\langle u\rangle_t$ term also modifies the vorticity flux at the wall.

wall region of the flow over an impermeable boundary [6, 7], are inappropriate here and the relevant form of the equations is that for which molecular effects are ignorable. By applying the jump conditions across the layer, δy, in which the jets "mix out," the following expressions for the turbulence kinetic energy and isotropic dissipation ensue:

$$\rho t \delta k = \delta q_k + |P_k - D_k| \delta y, \quad \text{and} \tag{12}$$

$$\rho t \delta \epsilon = \delta q_\epsilon + |P_\epsilon - D_\epsilon| \delta y, \tag{13}$$

where $|\ |$ indicates the vertical spatial average across the δy layer and the diffusive fluxes (q), production (P) and dissipation (D) are:

$$\begin{aligned} q_k &= (\mu_t/\sigma_k)\partial k/\partial y, & q_\epsilon &= (\mu_t/\sigma_\epsilon)\partial \epsilon/\partial y \\ P_k &= \mu_t (\partial u/\partial y)^2, & P_\epsilon/\epsilon &= C_1 \times P_k/k \\ D_k &= \epsilon, & D_\epsilon/\epsilon &= C_2 \times D_k/k \end{aligned} \tag{14}$$

Utilizing expressions or values for μ_t ($C_\mu \rho k^2/\epsilon$), σ_k, σ_ϵ, C_1, and C_2, the magnitudes of k and ϵ at δy may be computed in terms of k and ϵ injected through the boundary and the near wall profiles. Therefore, the formalism by which the external flow responds to the strucutre of the injected flow, which was observed earlier for nonturbulent vortical details, carries over to turbulence as well.

Note that, for flows with streamwise pressure gradients, injection of material which undergoes a phase change at the boundary complicates the discussion of injected vortical structure due to the $\nabla\langle p\rangle \times \nabla\langle\rho\rangle^{-1}$ vorticity generation effect. In addition, dilatation effects may be important if either phase is compressible. Finally, for integral formulation, the standard mass transfer term is modified to: $(1 - \langle u\rangle_w/u_e)$ $(\langle r\rangle_w/u_e)$ and $\langle u^0 v^0\rangle$ and the Reynolds stresses (if the flow is turbulent) at the wall are included. Utilizing such a formulation, the effects of slip/vectoring and the peculiarities of various walls on $\langle u^0 v^0\rangle$ may be examined with data such as that in reference [8].

Acknowledgment

This work was carried out under the sponsorship of the Aerospace Sciences Directorate, AFOSR and the Office of Basic Energy Sciences, Department of Energy.

References

1 Beavers, G. S., and Joseph, D. D., "Boundary Conditions at a Naturally Permeable Wall," *JFM*, 196?, Vol. 30, Part 1, pp. 197-207.

2 Taylor, G. I., "A Model for the Boundary Condition of a Porous Material," Part 1, *JFM*, 1971, Vol. 49, Part 2, pp. 319-336.

3 Saffman, P. G., "On the Boundary Condition at the Surface of a Porous Medium," *Studies in Applied Mathematics*, Vol. 1, No. 2, June 1971, pp. 93-101.

4 Hokenson, G. J., "Boundary Conditions with Heat/Mass Transfer and Velocity Slip," *AIAA Journal*, Vol. 15, No. 3, March 1977, pp. 438-439.

5 Kutateladze, S. S., and Leont'ev, A. I., *Boundary Layers in Compressible Gases*, tranlated by D. B. Spalding, Academic Press, New York, 1964.

6 Jones, W. P., and Launder, B. E., "The Prediction of Laminarization with a Two-Equation Model of Turbulence," *International Journal of Heat and Mass Transfer*, Pergamon Press, London, England, Vol 15, 1972, pp. 301-314.

7 Chien, K.-Y., "Predictions of Channel and Boundary-Layer Flows with a Low-Reynolds-Number Turbulence Model," *AIAA Journal*, Vol. 20, No. 1, Jan. 1982, pp. 33-38.

8 Collier, Jr., F. S., and Schetz, J. A., "Injection into a Turbulent Boundary Layer Through Different Porous Surfaces," *AIAA Journal*, Vol. 22, No. 6, June 1984, pp. 839-841.

Vorticity with Variable Viscosity

G. J. Hokenson

Reprinted from AIAA Journal Volume 24, Number 6, June 1986, Page 1039

AMERICAN INSTITUTE OF AERONAUTICS AND ASTRONAUTICS • 1633 BROADWAY • NEW YORK, N.Y. 10019

Vorticity with Variable Viscosity

Gustave J. Hokenson*
The Hokenson Company, Los Angeles, California

THE formulations developed in Ref. 1 are eminently useful in the analysis of vorticity mechanics in complex flows. As noted therein, the focus of the study was not viscous compressible flow. However, some of the equations retain the viscosity inside various derivatives, implying that all the variable viscosity effects are accounted for, at least formally. The purpose of this Note is to document some effects of the additional terms required to complete the formulation when variable viscosity flow is the subject of interest.

Following the notation in Ref. 2, the equations of motion may be written in the following form:

$$\rho Du_i/Dt = \rho F_i - \frac{\partial p}{\partial x_i} + \frac{\partial}{\partial x_j}\left\{2\mu\left(e_{ij} - \frac{1}{3}\Delta\delta_{ij}\right)\right\} \qquad (1)$$

where e_{ij} is the symmetric part of the deformation

$$e_{ij} = \frac{(\partial u_i/\partial x_j + \partial u_j/\partial x_i)}{2} \qquad (2)$$

$\Delta = e_{ij}$ and δ_{ij} is the Kronecker delta. Density, vorticity, velocity, normal stress, body force, and the coefficient of viscosity are assigned their traditional nomenclature.

Submitted June 7, 1985; revision received Sept. 21, 1985.

*Chief Scientist. Member AIAA.

Straightforward differentiation of the viscous terms in Eq. (1) allows them to be written

$$\mu\left(\nabla^2 u_i + \frac{\partial\Delta/\partial x_i}{3}\right) + \frac{2(e_{ij}\partial\mu/\partial x_j - \Delta\partial\mu/\partial x_i)}{3} \tag{3}$$

In addition, the appropriate vector calculus identity allows this expression to be rewritten as

$$-\mu(\nabla\times\omega)_i + \frac{4}{3}\frac{\mu\partial\Delta}{\partial x_i} + 2\left(e_{ij}\frac{\partial\mu}{\partial x_j} - \frac{\Delta\partial\mu}{\partial x_i}\right) \tag{4}$$

In order to derive the vorticity transport equation, this expression is substituted into the equations of motion, each term is divided by density ρ, and the entire expression is subjected to the curl operator. Comparing this with Eq. (1) in Ref. 1, it is clear that the additional variable viscosity terms

$$2\nabla\times\frac{(e_{ij}\partial\mu/\partial x_j - \Delta\partial\mu/\partial x_i)}{\rho} \tag{5}$$

must be addressed for general viscous flows.

The focus of interest in this study is the effect of the first term in flows for which the approximation $\rho \simeq$ constant, $\Delta \simeq 0$ is a good one, yet μ must be allowed to vary. In addition to various laminar flows, this situation is applicable to turbulence modeling as well, in which μ is related to the local flowfield properties. We consider, therefore, the following term in the general vorticity transport balance:

$$\left(\frac{2}{\rho}\right)\nabla\times\left(e_{ij}\frac{\partial\mu}{\partial x_j}\right) \tag{6}$$

For cases of interest in which μ varies predominantly in one direction, herein x_2, the components of the curl in the three orthogonal directions are

$$\begin{aligned}
&\frac{\partial}{\partial x_2}\left(\frac{e_{12}\partial\mu}{\partial x_2}\right) - \frac{\partial}{\partial x_3}\left(\frac{e_{22}\partial\mu}{\partial x_2}\right); \quad x_1\\
&\frac{\partial}{\partial x_3}\left(\frac{e_{32}\partial\mu}{\partial x_2}\right) - \frac{\partial}{\partial x_1}\left(\frac{e_{12}\partial\mu}{\partial x_2}\right); \quad x_2\\
&\frac{\partial}{\partial x_1}\left(\frac{e_{22}\partial\mu}{\partial x_2}\right) - \frac{\partial}{\partial x_2}\left(\frac{e_{12}\partial\mu}{\partial x_2}\right); \quad x_3
\end{aligned} \tag{7}$$

If x_1, x_2, and x_3 are associated with the streamwise, normal, and spanwise coordinates of a shear flow, it is clear that explicit three-dimensionality is required to impact streamwise vorticity from variable viscosity terms. However, in two-dimensional flow, the spanwise vorticity is affected by the component of the curl in x_3:

$$\frac{\partial\mu}{\partial x_2}\left(\frac{\partial e_{22}}{\partial x_1} - \frac{\partial e_{12}}{\partial x_2}\right) - \frac{\partial^2\mu}{\partial x_2^2}e_{12} \tag{8}$$

which may be written

$$\frac{\partial\mu}{\partial x_2}\left(\frac{\partial}{\partial x_2}\frac{\omega_3}{2}\right) - \frac{\partial^2\mu}{\partial x_2^2}e_{12} \tag{9}$$

If, in addition, $u_2 \ll u_1$, this expression further reduces to one-half of

$$\frac{\partial\mu}{\partial x_2}\left(\frac{\partial}{\partial x_2}\frac{\partial u_1}{\partial x_2}\right) - \frac{\partial^2\mu}{\partial x_2^2}\frac{\partial u_1}{\partial x_2} \tag{10}$$

or

$$\frac{\partial\mu}{\partial x_2}\frac{\partial^2 u_1}{\partial x_2^2} - \frac{\partial^2\mu}{\partial x_2^2}\frac{\partial u_1}{\partial x_2} \tag{11}$$

If, for example, μ exhibits some empirical dependence on, say, $\partial u_1/\partial x_2$, the vorticity generation will respond to a term proportional to

$$\mu\frac{\partial^2\mu}{\partial x_2^2} - \left(\frac{\partial\mu}{\partial x_2}\right)^2 \tag{12}$$

which, clearly, can undergo several sign changes across a shear flow and contribute positive or negative terms to the vorticity balance. The accurate representation of variable viscosity effects is, therefore, critical in representing the detailed vortical mechanics.

Acknowledgment

This work was carried out under the sponsorship of the Aerospace Sciences Directorate, Air Force Office of Scientific Research.

References

[1] Lakshminarayana, B. and Horlock, J. H., "Generalized Expressions for Secondary Vorticity Using Intrinsic Co-ordinates," *Journal of Fluid Mechanics*, Vol. 59, Pt. 1, 1973, pp. 97-115.

[2] Batchelor, G. K., *An Introduction to Fluid Dynamics*, Cambridge University Press, 1970, p. 147.

Thrust Vector Control Utilizing Asymmetric Jet Nozzles

G.J. Hokenson

Reprinted from
Journal of Spacecraft and Rockets Volume 23, Number 6, November-December 1986, Page 6
AMERICAN INSTITUTE OF AERONAUTICS AND ASTRONAUTICS • 1633 BROADWAY • NEW YORK, N.Y. 10019

Thrust Vector Control Utilizing Asymmetric Jet Nozzles

Gustave J. Hokenson*
The Hokenson Company, Los Angeles, California

RECENTLY interest in thrust vector control with rigidly mounted thrusters has been revived. The results described in this Note are associated with the side-force generated by a supersonic jet with an exit plane which is oblique to the centerline of the exhaust flow. As shown in Fig. 1, depending on whether the flow is over- or under-expanded, the direction of the exhaust flow is deflected either toward or away from the normal to the exit plane by an amount related to the pressure imbalance and the projected area of the exit plane in the lateral direction.[1] Therefore, control over the direction and amount of side-force is available by varying the stagnation pressure and exit plane obliquity.

Although the present results are associated with a two-dimensional configuration, with the exit plane obliquity established by extending one wall of the nozzle, application to an axisymmetric configuration is conceivable. For example, consider a fixed axisymmetric thruster enclosed by a cylindrical housing which is split longitudinally into various sections (see Fig. 1). At the null position, the end of the cylinder coincides with the exit plane of the thruster. As various combinations of cylindrical sections are translated forward of the exit plane, the radially projected area of the exit plane may be oriented toward any azimuthal angle. The amount of projected area and its orientation may also be changed rapidly, which adds another control feature to the thrust vectoring.

The focus of the work described in Ref. 2 involved the extent to which viscous effects affected the performance, particularly at over-expanded conditions. A two-dimensional supersonic jet of aspect ratio (height/width) equal to 1.5 was established over the Mach number range 1.0 to 3.0. One wall of the nozzle contour was then extended a specified fraction of the nozzle height to establish an oblique exit plane. Transparent and parallel lateral sidewalls bounded the nozzle and extensions thereof through which the flow angle could be observed. The side force generated was measured with a strain gage balance to an accuracy of ±2% of the reading, based on the scatter in repeated experiments and comparison to the measured flow angle.

In order to assess the degree to which viscous effects impede accurate analytical prediction, the amount of asymmetry was limited to maintain the wall extension within the domain established by the Mach wave originating from the opposite nozzle wall at the exit plane.

Figures 2-4 depict the forces measured on three nozzles whose exit plane is offset by an amount 1.0, 4/3, and 5/3 times the jet height, respectively. Comparison with predictions of two-dimensional inviscid flow theory is shown also. These results may be converted into force coefficients by dividing the results by the surface area of the wall extension and the exit dynamic pressure. The corresponding plot of the Fig. 3 data is presented in Fig. 5. These results indicate that, even in the simple case established here, nontrivial deviations between inviscid flow theory and experiment are observed, although the general trends predicted by analysis are correct. It is also clear that the vectoring control may extend well into the over-expanded region before the nozzle boundary layers begin to

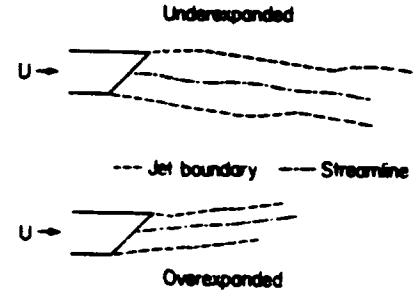

Fig. 1 Configuration of the nozzle, jet boundary, and center streamline for two-dimensional (and a longitudinal slice of an azimuthally varying axisymmetric nozzle) flow in under- and over-expanded conditions.

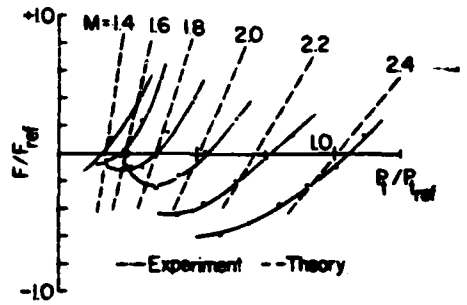

Fig. 2 Side-force vs stagnation pressure for various Mach numbers on a two-dimensional supersonic jet nozzle with an asymmetric exit plane. Asymmetry factor (nozzle wall extension/nozzle exit height) = 1.0, F_{ref} = 0.5 lb, $P_{t_{ref}}$ = 200 psig.

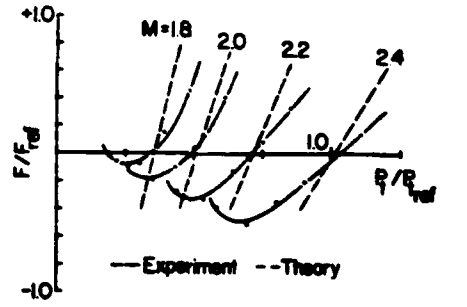

Fig. 3 Side-force vs stagnation pressure for various Mach numbers on a two-dimensional supersonic jet nozzle with an asymmetric exit plane. Asymmetry factor (nozzle wall extension/nozzle exit height) = 4/3, F_{ref} = 0.5 lb, $P_{t_{ref}}$ = 200 psig.

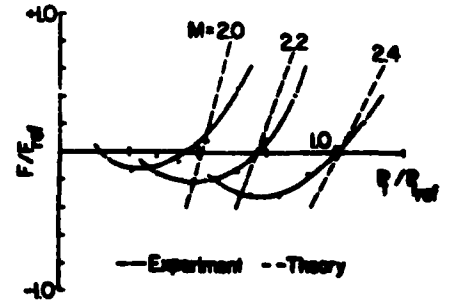

Fig. 4 Side-force vs stagnation pressure for various Mach numbers on a two-dimensional supersonic jet nozzle with an asymmetric exit plane. Asymmetry factor (nozzle wall extension/nozzle exit height) = 5/3, F_{ref} = 0.5 lb, $P_{t_{ref}}$ = 200 psig.

Received Sept. 16, 1985; revision received Nov. 18, 1985.

*Chief Scientist. Member AIAA.

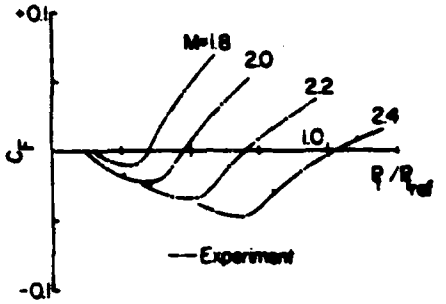

Fig. 5 Side-force coefficient vs stagnation pressure for various Mach numbers for the data from Fig. 2. Reference area and pressure are the lateral projected area of the asymmetry and the exit dynamic pressure.

separate and the entire flow degrades, although the Reynolds number dependence of the effect in this configuration remains to be quantified. On the basis of these data, it is concluded that control of the thruster plenum pressure and exit plane obliquity (including the aforementioned axisymmetric case wherein the sideforce vector may be oriented azimuthally) provides the ability to quickly orient the thrust vector of nongimballed jets.

Acknowledgments

The data in Ref. 2 were acquired while the author was on the faculty of the Department of Aeronautics at the U.S. Naval Postgraduate School. Preparation of this paper was supported by the Aerospace Sciences Directorate of AFOSR and the Office of Basic Energy Sciences, Department of Energy.

References

[1]Ferri, A., *Elements of Aerodynamics of Supersonic Flows*, The Macmillan Company, 1949, pp. 170-172.

[2]Horais, Brian J., "Vectored Thrust Control," MS Thesis, U.S. Naval Postgraduate School, Monterey, CA, Dec. 1972.

Appendix B

DRAFT OF FUTURE PUBLICATION

The angular structure of viscous incompressible flow

Part I. Analysis

Gustave J. Hokenson, Chief Scientist
The Hokenson Company
Los Angeles, CA 90005

Abstract

The governing equations for time-dependent three-dimensional viscous shear flows are transformed into velocity vector angle and magnitude variables to expose the flow angle structure in various limiting situations. For purposes of analysis when the mean streamwise flow is reasonably well characterizable, this formulation admits the possibility for extracting essential flowfield peculiarities and providing insight into various complex interactions, including those associated with turbulent flow. For full numerical simulations of shear flows, the formulation simplifies the mathematical structure and may allow for more effective computation.

I. Introduction

The use of velocity vector magnitude and angle variables in the solution of inviscid compressible and incompressible flows has a long history of successful application.[1,2] Less common is the implementation of such an approach in viscous shear flows, which is the subject of this study. Part I of the work involves an exposition of the general formulation and its application in various limiting cases. In a future paper, the results of a computational study, which has been initiated, shall be presented.

Consider the time-dependent three-dimensional continuity and Navier-Stokes equations for a constant density Newtonian fluid[3]:

$$u_x + v_y + w_z = 0 \quad , \tag{1}$$

$$\begin{aligned} u_t + (u^2)_x + (uv)_y + (uw)_z &= F \\ v_t + (vu)_x + (v^2)_y + (vw)_z &= G \\ w_t + (wu)_x + (wv)_y + (w^2)_z &= H \quad , \end{aligned} \tag{2}$$

where:

$$\begin{aligned} F &\equiv - p_x + \nu\nabla^2 u \\ G &\equiv - p_y + \nu\nabla^2 v \\ H &\equiv - p_z + \nu\nabla^2 w \quad , \end{aligned} \tag{3}$$

and ν is the constant kinematic viscosity, ∇^2 the conventional Laplacian operator and p is defined as the mean normal stress (herein equated to the equilibrium thermodynamic pressure) divided by density. Following conventional terminology u,x; v,y; w,z correspond to the nominal streamwise, normal (along which the dominant velocity gradients occur), and spanwise velocities and coordinates, respectively.

The following dependent variables are now introduced in an attempt to expose the angular structure of various shear flows:

$$m \equiv (u^2 + v^2 + w^2)/u^2_{(r)}$$

$$\Theta \equiv v/u \qquad (4)$$

$$\alpha \equiv w/u \quad ,$$

where $u_{(r)}$ is an appropriate reference velocity. In general, we do not expect this transformation to be useful when the streamline lies in the (y-z) plane orthogonal to the nominal streamwise (x) direction. That is, when u=0 but v,w $\neq$ 0 we may have to retreat from this formulation, locally.

Clearly, m may be expressed as:

$$m = (u/u_{(r)})^2 \ (1 + \Theta^2 + \alpha^2) \quad . \qquad (5)$$

For convenience in transforming the equations, several of these terms are grouped together such that u may be written:

$$u^2 = m\beta \; ; \; \beta^{-1} \equiv (1 + \Theta^2 + \alpha^2)/u^2_{(r)} \quad . \tag{6}$$

Utilizing these definitions and relationships for m, Θ and α, Eqs. (3) become:

$$(m\beta)^{\frac{1}{2}}_t + (m\beta)_x + (m\beta\Theta)_y + (m\beta\alpha)_z = F \tag{7}$$

$$((m\beta)^{\frac{1}{2}}\Theta)_t + (m\beta\Theta)_x + (m\beta\Theta^2)_y + (m\beta\alpha\Theta)_z = G \tag{8}$$

$$((m\beta)^{\frac{1}{2}}\alpha)_t + (m\beta\alpha)_x + (m\beta\alpha\Theta)_y + (m\beta\alpha^2)_z = H \quad . \tag{9}$$

By expanding the differentiation in Eqs. 8 and 9 and utilizing Eq. 7, the following compact, yet complete, relationships for Θ and α ensue:

$$N_{3t}\,\Theta = (G - \Theta F)/u \tag{10}$$

$$N_{3t}\,\alpha = (H - \alpha F)/u \quad , \tag{11}$$

where:

$$N_{3t} \equiv \partial/\partial t + u\,(\partial/\partial x + \Theta\partial/\partial y + \alpha\partial/\partial z) \quad . \tag{12}$$

Note that Eqs. 10 and 11 may be combined to express the sum and difference of the two flow angles in the following form:

$$N_{3t}\,(\Theta \pm \alpha) = \{(G \pm H) - F(\Theta \pm \alpha)\}/u \quad . \tag{13}$$

Clearly, continuity and the magnitude, m, momentum equation must be considered in order to provide a closed set of equations for u,v,w and p. They shall, indeed, be addressed later in this analysis but the focus of the work in Part I is to expose the structure of α and Θ for various cases in which u can be characterized parametrically. This approach embodies the dynamics of interest in lieu of the simple kinematics derivable from continuity if sufficient information on the streamwise and cross-stream derivatives is given.

Prior to addressing various specific cases, the form of the governing equations encourages us to examine the loci where $u = 0$. As long as the flow remains incompressible, this mathematical structure is complete and Θ, α and their derivatives are everywhere bounded within the previously-stated restriction of streamlines from the y-z plane. (It has been found that several important cases of interest satisfy this restriction when analyzed in detail but do not in traditional formulations. An example is a boundary layer with wall mass transfer. Clearly, at the wall $v \neq 0$ but u is traditionally set equal to zero. It is now known that u at the wall is small but finite[4,5].) Therefore, when $u = 0$, $N_{3t} = \partial/\partial t$, $\Theta = G/F$ and $\alpha = H/F$ with the values of $(G - \Theta F)/u$ and $(H - \alpha F)/u$ determined from L'Hospital's rule. If, in addition, $u = u_y = 0$, as occurs at the point of separation in a wall-bounded shear flow, $G - \Theta F$ and $H - \alpha F$ values are stationary at that point (still possibly zero) and the values of $(G - \Theta F)/u$ and $(H - \alpha F)/u$ are determined from the curvatures of $G - \Theta F$ and $H - \alpha F$. For various cases $G - \Theta F$ and $H - \alpha F$ may be either maxima or minima and, therefore, $\partial\alpha/\partial t$ and $\partial\Theta/\partial t$ may be positive or negative. Subsequently, we shall analyze specific steady flows which modify this argument somewhat.

II. Discussion

We now consider some restricted cases of the governing equations in more detail.

A. Steady Two - Dimensional Flow

In this situation, $\alpha = H = 0$ and the governing Θ equation becomes:

$$\Theta_x + \Theta\Theta_y = (G - \Theta F)/u^2 \quad , \tag{14}$$

or, in streamfunction (ψ, x) variables:

$$\Theta_x = (G - \Theta F)/u^2 \quad . \tag{15}$$

Within the same constraints as before ($\Theta \neq \infty$ by restriction and Θ_x, $\Theta_y \neq \infty$ by assumption of physicality), when $u = 0$, $\Theta = G/F$ but also, $G - \Theta F$ is stationary at zero. If, in addition, $u_y = 0$, $G - \Theta F$ and its first three derivatives must be zero. This is clearly a significantly strengthened constraint from its unsteady flow counterpart.

Utilizing the definitions of F and G along with the angle/magnitude transformation, the Θ equation may be written:

$$(1 - 2\nu(m\beta)^{\frac{1}{2}}_x/m\beta)\Theta_x + (\Theta - 2\nu(m\beta)^{\frac{1}{2}}_y/m\beta)\Theta_y = (-p_y + \Theta p_x)/m\beta + \nu\nabla^2\Theta/(m\beta)^{\frac{1}{2}}. \tag{16}$$

In order to isolate certain cases of interest, it is convenient to non-dimensionalize this equation with length scales $L_{(x)}$ and $L_{(y)}$, angle scale $\Theta_{(r)}$ and the previous velocity scale $u_{(r)}$. Utilizing the following definitions:

$$\lambda \equiv L_{(y)}/L_{(x)}$$

$$\Phi_{(x)} \equiv 2u_x/u^2$$

$$\Phi_{(y)} \equiv 2u_y/u^2 \qquad (17)$$

$$Re \equiv u_{(r)}L_{(x)}/\nu$$

$$\epsilon \equiv Re^{-1} \quad ,$$

the governing Θ equation in dimensionless variables becomes:

$$(1 - \epsilon\Phi_{(x)})\Theta_x + (\Theta - \epsilon\Phi_{(y)}/\lambda\Theta_{(r)})(\Theta_{(r)}/\lambda)\Theta_y = (\Theta p_x - p_y/\lambda\Theta_{(r)})/u^2 + \epsilon(\Theta_{xx} + \Theta_{yy}/\lambda^2)/u \quad . \qquad (18)$$

In order to retain the two-dimensional equation of *continuity* in its primitive form, λ is set equal to $\Theta_{(r)}$ so that the Θ equation may be written:

$$(1 - \epsilon\Phi_{(x)})\Theta_x + (\Theta - \epsilon\Phi_{(y)}/\lambda^2)\Theta_y = (\Theta p_x - p_y/\lambda^2)/u^2 + \epsilon(\Theta_{xx} + \Theta_{yy}/\lambda^2)/u \quad . \qquad (19)$$

We now consider various cases of interest for which $\epsilon << 1$. The most straightforward limit is $\lambda >> 1$ for which the first order solution for Θ (in an implied perturbation expansion) may be developed by letting $\lambda \to \infty$ in Eq. 19, resulting in:

$$\Theta_x + \Theta\Theta_y = \Theta p_x/u^2 + \epsilon\,\Theta_{xx}/u \quad , \qquad (20)$$

which can be made formally invariant with respect to ϵ by utilizing x/ϵ and y/ϵ as independent variables.

If, on the other hand, $\lambda << 1$ such that $\epsilon/\lambda^2 << 1$, i.e. λ is small relative to one but still large relative to the presumed very small ϵ, the governing θ equation becomes:

$$\theta_x + \theta\theta_y = - p_y/u'^2 + \epsilon'\theta_{yy}/u' \quad , \tag{21}$$

where:

$$u' \equiv \lambda u \quad , \text{ and}$$
$$\epsilon' \equiv \epsilon/\lambda \quad , \tag{22}$$

are used to maintain the canonical form of Eq. 20 which is independent of λ. Evidently, the appropriate velocity in this case is a typical v. Eq. 21 also may be made invariant with respect to ϵ via x/ϵ' and y/ϵ'.

This case is to be contrasted with the traditional boundary layer limit for which $\lambda << 1$ but $\epsilon/\lambda^2 = O(1)$ (i.e. $L_y/L_x \sim Re^{-\frac{1}{2}}$) so that all the coefficients in Eq. 19 are of order unity. If $\epsilon = O(\lambda^2)$, the term $- \Phi_{(y)}\, \theta_y$ must be retained and the equation becomes:

$$\theta_x + (\theta - (\epsilon/\lambda^2)\, \Phi_{(y)})\theta_y = - p_y/\lambda^2 u^2 + (\epsilon/\lambda^2)\theta_{yy}/u \quad . \tag{23}$$

For purposes of analysis, $-\Phi_{(y)}$ is treated as a small (variable viscosity - like) term which can be incorporated as a perturbation correction to the solution of:

$$\theta_x + \theta\theta_y = - p_y/u'^2 + \epsilon^{\frac{1}{2}}\theta_{yy}/u' \quad , \tag{24}$$

which is essentially identical to Eq. 21, except that $\epsilon' \equiv \epsilon/\lambda = \epsilon^{\frac{1}{2}}$. Eq. 24 also may be made invariant with respect to ϵ by employing $x/\epsilon^{\frac{1}{2}}$ and $y/\epsilon^{\frac{1}{2}}$ as independent variables.

The traditional use of Eqs. 21 and 24 involves the formal limit $\lambda \to 0$ for which $p_y \approx 0$, the boundary layer assumption. Note that the behavior in this limit is formally the same as our previous analysis of $u = 0$.

Our use of the previous scaling is directed at simplifying the coefficients in the governing equation while retaining all the terms such that the mathematical structure is complete. We leave it to the solution to expose the behavior of the dependent variables when ϵ and λ are small enough to have allowed various terms in the equation to be neglected.

Further analysis of Eq. 24 is facilitated by the use of streamfunction independent variables (ψ,x) which allows the equation to be written:

$$\Theta_x = - p_\psi/u' + \epsilon^{\frac{1}{2}} (u'\Theta_\psi)_\psi \quad . \qquad (25)$$

If we define an equilibrium, $\Theta_{(eq.)}$, which is independent of x, its distribution in terms of u' and p is:

$$\epsilon^{\frac{1}{2}}\Theta_{(eq.)} = \int 1/u' \int dp/u' \, d\psi + C_1\psi + C_2 \quad , \qquad (26)$$

which, if u' varies weakly with ψ (as it must in order to account for $\Phi_{(y)}$ via perturbation theory), reduces Eq. (26) to:

$$\epsilon^{\frac{1}{2}}\Theta_{(eq.)} \simeq (\int p d\psi)/u'^2 + C_1\psi + C_2 \quad . \tag{27}$$

In addition, thin internal layers may exist within the shear flow for which Eq. (25) provides the following 'jump' (δ) condition:

$$\int dp/u' = \epsilon^{\frac{1}{2}}\delta(u'\Theta_\psi) \quad , \tag{28}$$

or, for weakly varying u':

$$\epsilon^{\frac{1}{2}}\delta\Theta_\psi = \delta p/u'^2 \quad . \tag{29}$$

Finally, the general solution of Eq. (25), in terms of a known or characterizable p and u' field, is readily obtained from transient heat conduction solutions to the equation written as:

$$\Theta_x - \epsilon^{\frac{1}{2}}(u'\Theta_\psi)_\psi = - p_\psi/u' \quad , \tag{30}$$

and the u' (ψ) variations treated perturbatively and parametrically. In addition, since the u' (ψ) variations are weak in order to treat $\Phi_{(y)}$ via perturbations, u' may be set equal to a constant determined by collocation in order to optimize the approximation of neglecting its distribution.

If u' (Θ) characterizations are meaningful, Eq. 30 may be written:

$$\Theta'_x - \epsilon^{\frac{1}{2}}u'\,\Theta'_{\psi\psi} = - p_\psi \quad , \tag{31}$$

where: $$u'd\Theta = d\Theta' \quad ,$$

which, although non-linear, is particularly convenient for analysis. The 'equilibrium' solution and 'jump' conditions of Eq. (31) are apparent.

Analysis of the behavior of Eq. 20 is more clearly carried out computationally inasmuch as the conventional streamfunction (ψ,x) transformation results in a complex elliptic equation for Θ. If the less conventional (ψ,y) streamfunction transformation is invoked ($\partial/\partial x = -v\partial/\partial\psi$; $\partial/\partial y = \partial/\partial y + u\partial/\partial\psi$), Eq. 20 may be written in terms of $\Theta^2/2 \equiv \vartheta$:

$$\vartheta_y = -2\vartheta\, p_\psi/u + \varepsilon(2\vartheta)^{\frac{1}{2}}\,(u\vartheta_\psi)_\psi \quad , \tag{32}$$

in which the non-linearities limit closed form analysis. However, the equilibrium and 'jump' conditions may be approached as before, particularly if u (ϑ) relationships (where $ud\vartheta = d\vartheta'$) are useful.

B. Steady Three - Dimensional Flow

By expanding and non-dimensionalizing Eqs. 10 and 11, the following expressions for Θ and α ensue as $\varepsilon \to 0$:

$$\begin{aligned} &\Theta_x + (\Theta - (\varepsilon/\lambda^2_{(y)})\Phi_{(y)})\Theta_y + (\alpha - (\varepsilon/\lambda^2_{(z)})\Phi_{(z)})\Theta_z = \\ &-(p_y/\lambda^2_{(y)} - \Theta p_x)/u^2 + \varepsilon(\Theta_{xx} + \Theta_{yy}/\lambda^2_{(y)} + \Theta_{zz}/\lambda^2_{(z)})/u \end{aligned} \tag{33}$$

$$\begin{aligned} &\alpha_x + (\Theta - (\varepsilon/\lambda^2_{(y)})\Phi_{(y)})\alpha_y + (\alpha - (\varepsilon/\lambda^2_{(z)})\Phi_{(z)})\alpha_z = \\ &-(p_z/\lambda^2_{(z)} - \alpha p_x)/u^2 + \varepsilon(\alpha_{xx} + \alpha_{yy}/\lambda^2_{(y)} + \alpha_{zz}/\lambda^2_{(z)})/u \quad , \end{aligned}$$

where the additional scale ratio $\lambda_{(z)}$ ($\equiv L_{(z)}/L_{(x)}$) has been introduced and the characteristic angle, $\alpha_{(r)}$, has been set equal to $\lambda_{(z)}$ in order to retain continuity in its primitive form.

In the limit as $\lambda_{(y)}, \lambda_{(z)} \to \infty$, Eqs. (33) may be written:

$$\{\partial/\partial x + \Theta\partial/\partial y + \alpha\partial/\partial z - p_x/u^2 - (\epsilon/u)\partial^2/\partial x^2\}\,\Theta,\alpha = 0 \qquad .(34)$$

Alternatively, if $\lambda_{(y)} = \lambda_{(z)} \to 0$ such that ϵ/λ^2 is still small, Eqs. 33 become:

$$\{\partial/\partial x + \Theta\partial/\partial y + \alpha\partial/\partial z + p_j/u'^2 - (\epsilon'/u')(\partial^2/\partial y^2 + \partial^2/\partial z^2)\}\Theta,\alpha = 0, \qquad (35)$$

where $j = y$ for Θ and $j = z$ for α. In the traditional boundary layer limit this same form is retained with $\epsilon^{\frac{1}{2}}$ replacing ϵ' and the (presumed weak) variable viscosity - like Φ terms accounted for perturbatively. Clearly, if $\Phi_{(y)}$ and $\Phi_{(z)}$ are large, they must be included with Θ and α in the advective operator.

In the mixed limit case, $\lambda_{(z)} \to \infty$ and $\lambda_{(y)} \to 0$ such that $\epsilon/\lambda^2_{(y)} = 1$, Eqs. (33) become:

$$N_3\Theta = - p_y/u'^2 + \epsilon^{\frac{1}{2}}\,\Theta_{yy}/u'$$

$$N_3\alpha = \alpha p_x/u^2 + \alpha_{yy}/u \qquad (36)$$

where: $$N_3 \equiv \partial/\partial x + \Theta\partial/\partial y + \alpha\partial/\partial z \quad ,$$

and $\Phi_{(y)}$ must be accounted for at higher order. Alternatively, if $\lambda_{(y)} \to \infty$ and $\lambda_{(z)} \to 0$ such that $\epsilon/\lambda^2_{(z)} = 1$, the Eqs. (33) are written:

$$N_3\theta = \theta p_x/u^2 + \theta_{zz}/u$$

$$N_3\alpha = - p_z/u'^2 + \epsilon^{\frac{1}{2}}\alpha_{zz}/u' \quad , \tag{37}$$

again assuming that $\Phi_{(z)}$ is subsequently accomodated. By scrutinizing these mixed limit cases it is clear that the essential angular structure of the flow will be markedly different from that we have observed previously. Consider, for example, the case where $p_x = 0$ and α is small. This results in:

$$\theta_x + \theta\theta_y = \theta_{zz}/u \quad , \tag{38}$$

indeed a curious mix of derivatives. Three-dimensional phenomena are most clearly investigated numerically and will be described in a future publication. Note that, unlike two-dimensional flows, total knowledge of u is inadequate to prescribe the angular structure from the kinematics of the incompressible continuity equation.

C. Time - Dependent Flow

By adding the dimensional terms:

$$\theta_t/u \text{ and } \alpha_t/u \tag{39}$$

to the advective operators in Eqs. (33), the three-dimensional formulation embraces unsteady flows as well. After non-dimensionalization, these terms are scaled by a

coefficient:

$$L_{(x)}/t_{(r)}u_{(r)} \quad , \tag{40}$$

where $L_{(x)}$ replaces $\theta_{(r)}$ and $\alpha_{(r)}$ after clearing the equations with respect to $\theta_{(r)}/L_{(x)}$ and $\alpha_{(r)}/L_{(x)}$, respectively. If $t_{(r)}$ is chosen as $L_{(x)}/u_{(r)}$, the additional dimensionless terms θ_t/u and α_t/u are present in all equations for which $\lambda \to \infty$.

In cases for which $\lambda_{(y)} = \lambda_{(z)} \to 0$, it is more consistent, formally, to set $t_{(r)} = L_{(y,z)}/u_{(r)}$ and express the operators as:

$$\begin{aligned} &\theta_t/u' + \theta_x + \ldots\ldots \quad , \text{and} \\ &\alpha_t/u' + \alpha_x + \ldots\ldots \quad . \end{aligned} \tag{41}$$

For mixed limits, the α and θ equations respond most naturally with different 'time constants', significantly enriching the range of solution characteristics to be exposed numerically.

For the two-dimensional flow governed by Eq. (24), the unsteady counterpart is:

$$\theta_t/u' + \theta_x + \theta\theta_y = - p_y/u'^2 + \varepsilon^{\frac{1}{2}}\theta_{yy}/u' \quad , \tag{42}$$

or, in conventional streamfunction variables:

$$\theta_t + u'\theta_x = - p_\psi + \varepsilon^{\frac{1}{2}}u' \, (u'\theta_\psi)_\psi \quad . \tag{43}$$

If the transformation $d\vartheta = u'\, d\Theta$ allows for meaningful parameterization of the velocity field, Eq. (43) may be written:

$$\vartheta_t/u' + \vartheta_x = - p_\psi + \epsilon^{\frac{1}{2}} u'\, \vartheta_{\psi\psi} \quad , \tag{44}$$

both of which illustrate significant changes in the boundary layer approximation $p_\psi = 0$.

For purposes of analysis, if $u' = u'(\psi)$, along curves in the x - t plane for which x - u't is a constant, Eq. 43 may be written:

$$\Theta_t = - p_\psi + \epsilon^{\frac{1}{2}} u'\, (u'\Theta_\psi)_\psi \quad . \tag{45}$$

Once again, the general transient structure is so complex for either two- or three-dimensional flows as to require numerical investigation.

With regard to time-dependent flows, considerable interest exists relative to the angular structure of turbulent flows. The counterpart of the Reynolds stress tensor may be found by setting $\epsilon = 0$ in Eqs. (33). For notational simplicity, the case $\lambda_{(y)} = \lambda_{(z)} = \infty$ will be used without justification. In this case, the equations for Θ and α become:

$$\{u^{-1}\partial/\partial t + \partial/\partial x + \Theta\partial/\partial y + \alpha\partial/\partial z - p_x/u^2\}\ \alpha,\Theta = 0 \quad . \tag{46}$$

Since the continuity equation may be written:

$$u_x + (u\Theta)_y + (u\alpha)_z = 0 \quad , \tag{47}$$

Eqs. (46) become:

$$\alpha_t + (u\alpha)_x + (u\theta\alpha)_y + (u\alpha^2)_z = \alpha p_x/u \quad , \text{and}$$

$$\theta_t + (u\theta)_x + (u\theta^2)_y + (u\alpha\theta)_z = \theta p_x/u \quad . \tag{48}$$

If we consider two-dimensional "turbulence" in order to expose the angular Reynolds stresses, Eq. 48 may be written utilizing traditional Reynolds decomposition as:

$$\bar{\theta}_x + \bar{\theta}\bar{\theta}_y = \bar{\theta}\bar{P}/\bar{u}^2 - \bar{\theta}(\overline{P'u'} + (\overline{u'\theta'})_y)/\bar{u} - \overline{u'\theta'}(2\bar{\theta}_y + \bar{P})/\bar{u} - \overline{\theta'P'} \quad , \tag{49}$$

where $P \equiv p_x$ and triple correlations of the fluctuations (designated by the prime) and the x - derivative of $\overline{u'\theta'}$ have been neglected. In addition, the ensemble mean values (designated by the overbar) have been assumed to be time - independent. The term $(\overline{u'\theta'})_y$ is reminiscent of the conventional Reynolds shear stress. However, this formulation exposes additional explicit effects of $\bar{P}$, $\bar{\theta}$ and $\bar{\theta}_y$ and correlations between P', u' and θ'. It remains to be seen whether or not the explicit appearance of these various terms is sufficiently advantageous in light of the additional superficial complication.

With regard to the turbulent burst dynamics, various aspects of the vortical instabilities are often described in terms of a four quadrant u' - v' map.[6] Equations for θ' and its statistical characterization may also be derived from the full θ and $\bar{\theta}$ relationships, providing an analytical tool with which to quantify the various details which support the aforementioned four quadrant uniquenesses of turbulent burst dynamics.

III. Conclusion

The full time-dependent three-dimensional Navier - Stokes equations for incompressible viscous shear flows have been converted to vector angle and magnitude variables for analysis in various limiting cases. This dependent variable transformation, in conjunction with a streamfunction independent variable is seen to simplify the system of equations and permit analysis of the angular structure with the pressure and velocity field treated parametrically. The utility of this formulation in the study of turbulence appears to have merit. Finally, the equation structure is often considerably more "symmetric" in these variables and may facilitate numerical studies which are currently under way.

IV. References

1. M. Schiffer, Analytical Theory of Subsonic and Supersonic Flows, Handbuch der Physik, Bd. IV.

2. G.J. Hokenson, AIAA J., Vol. 15, pp. 39-45, 1977.

3. G.K. Batchelor, An Introduction to Fluid Dynamics, Cambridge University Press, 1970.

4. G.J. Hokenson, JFE, to be published, 1985.

5. Referring to Eqs. (2), it is clear that the vectoring of wall mass flux (natural or induced) and its time dependence, if any, are crucial to the understanding of the vorticity mechanics with mass transfer since the wall vorticity flux $\partial\omega/\partial y = -\nabla^2 u$.

6. W.W. Wilmarth, Structure of Turbulence in Boundary Layers, Adv. in App. Mech., Vol. 15, 1975.

Appendix C

TBL INSTABILITY COMPUTATION INPUTS AND RESULTS

Figs. C1 & C2. Input Mean Velocity and Eddy Viscosity Profiles and Their Derivatives.

THE HOKENSON COMPANY

Fig. C1

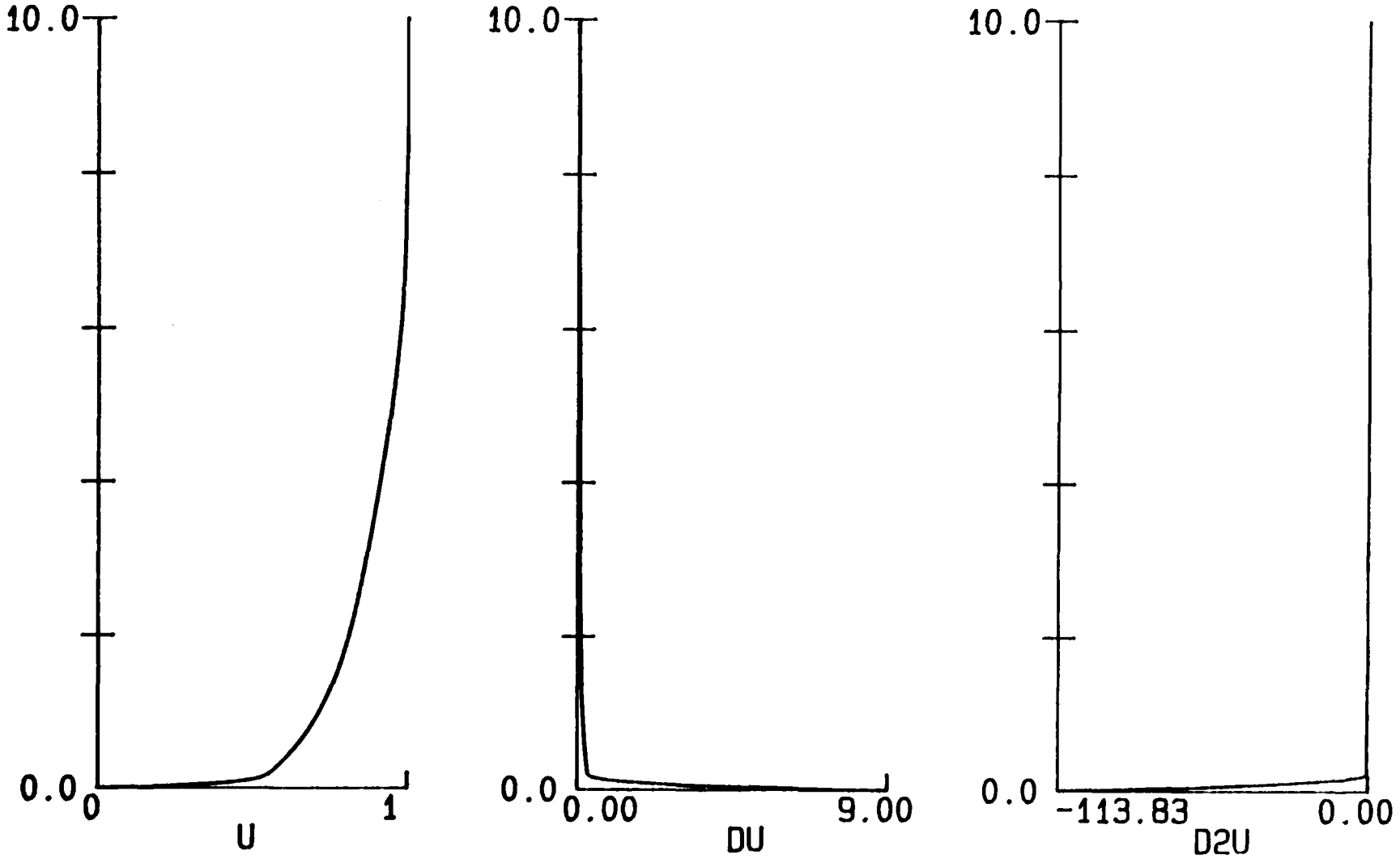

THE HOKENSON COMPANY

Fig. C2

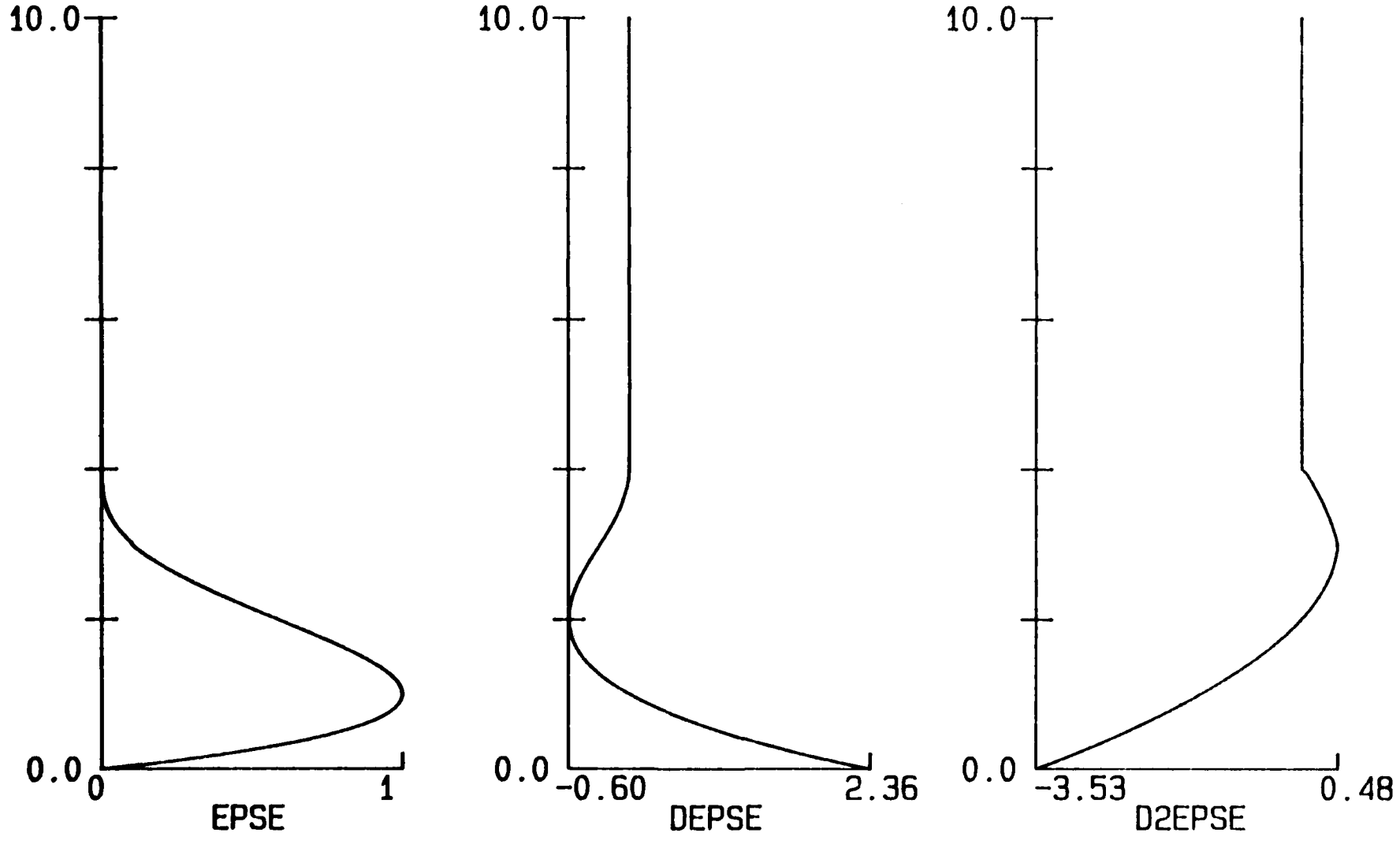

Fig. C3 & Table C3. Alpha Solutions For The Particular Case Shown.

THE HOKENSON COMPANY

Fig. C3

BETA 0.100
OMEGA 2.000
EPSMAG 1.000
TAUEPS 0.000
RE NO. 44369.

SOLUTIONS OF ALPHA

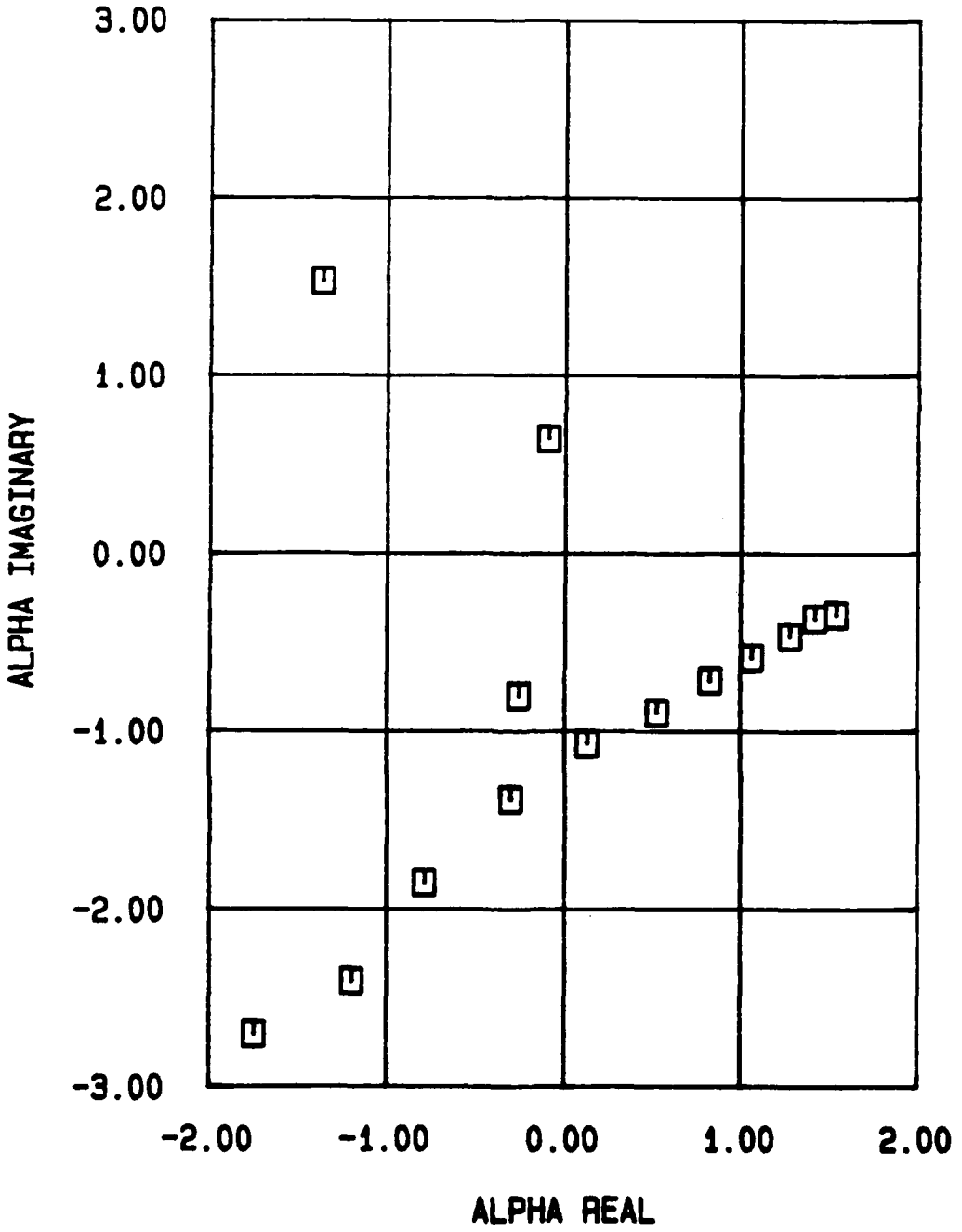

THE HOKENSON COMPANY

Table C3

BETA	0.100
OMEGA	2.000
EPSMAG	1.000
TAUEPS	0.000
RE NO.	44369.000

ALPHA REAL	ALPHA IMAGINARY	K	PHASE SPEED
-0.30270	-1.37840	4.55368	-6.60720
0.13009	-1.06779	-8.20811	15.37404
-0.25528	-0.79761	3.12447	-7.83455
-0.78500	-1.85000	2.35669	-2.54777
0.82936	-0.71168	-0.85811	2.41150
1.06350	-0.58185	-0.54711	1.88058
1.28000	-0.46000	-0.35938	1.56250
1.42000	-0.36000	-0.25352	1.40845
1.54000	-0.34000	-0.22078	1.29870
0.52391	-0.89511	-1.70851	3.81744
-1.19534	-2.40390	2.01106	-1.67316
-1.74600	-2.70400	1.54868	-1.14548
-0.09086	0.64849	-7.13706	-22.01140
-1.36535	1.53441	-1.12382	-1.46483

Figs. C4 - C10. Eigenfunctions For The Solution: $\alpha_r = .13$ and $\alpha_i = -1.07$ On Fig. C3.

THE HOKENSON COMPANY

Fig. C4

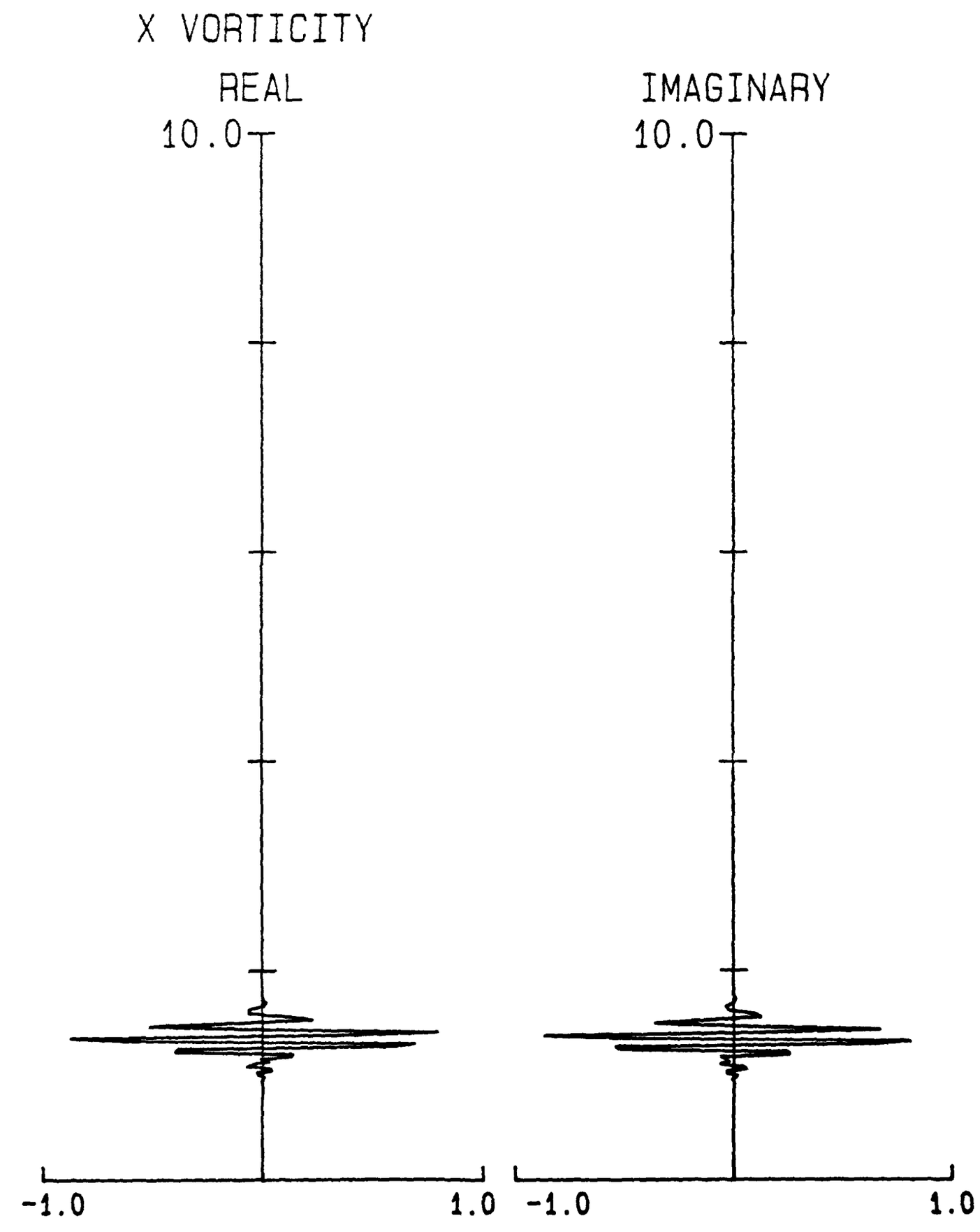

THE HOKENSON COMPANY

Fig. C5

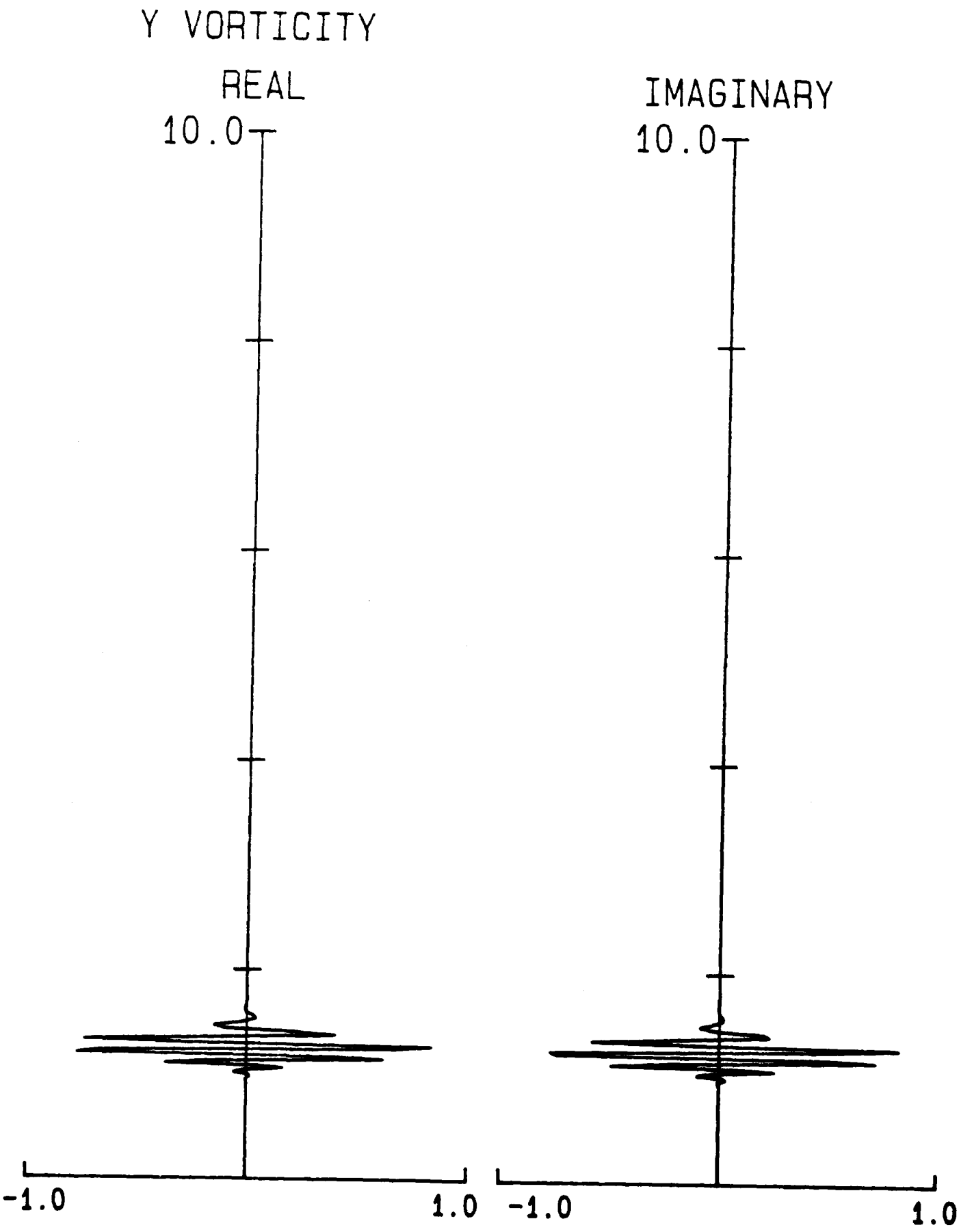

THE HOKENSON COMPANY

Fig. C6

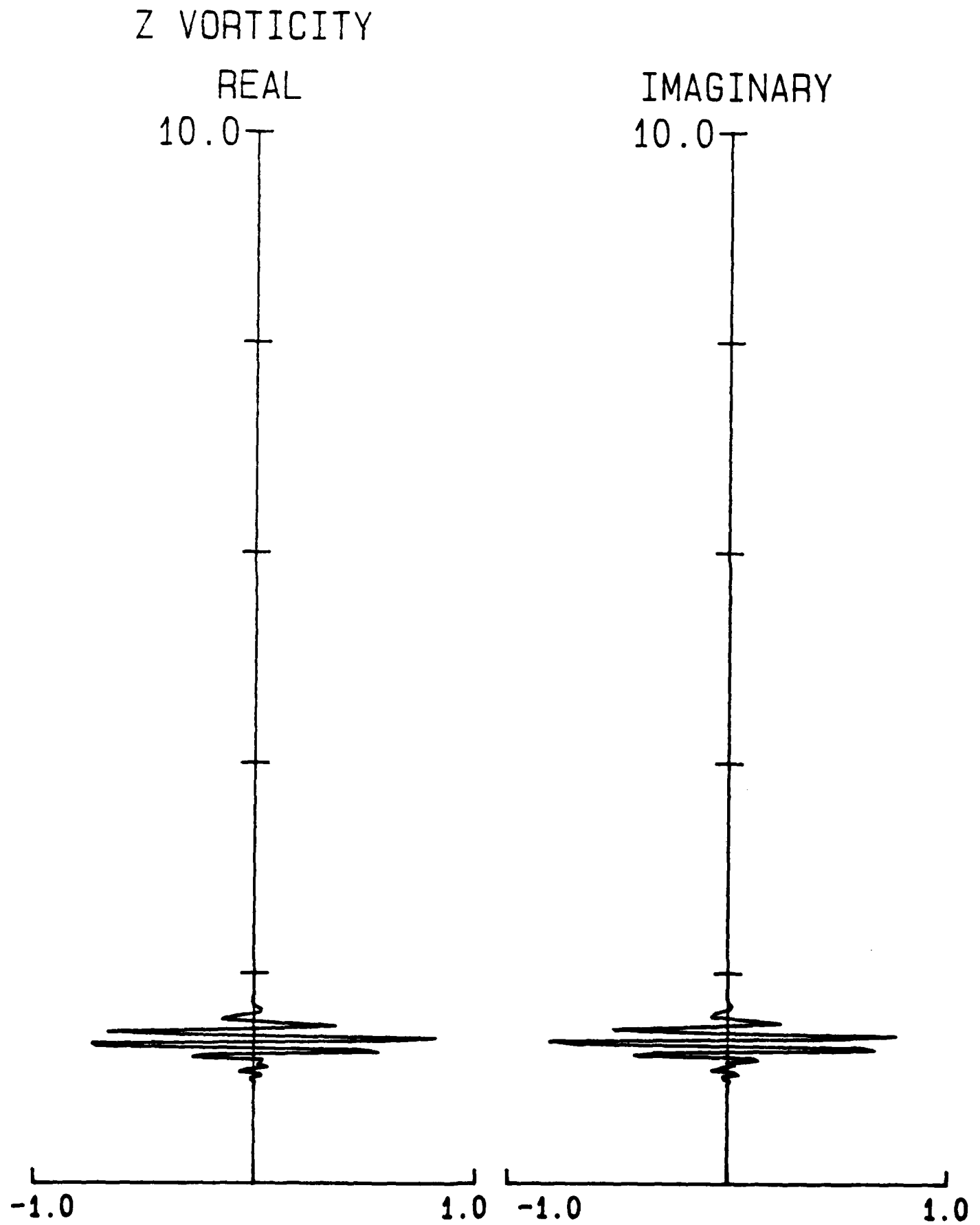

THE HOKENSON COMPANY

Fig. C7

PRESSURE STRESS PROFILE

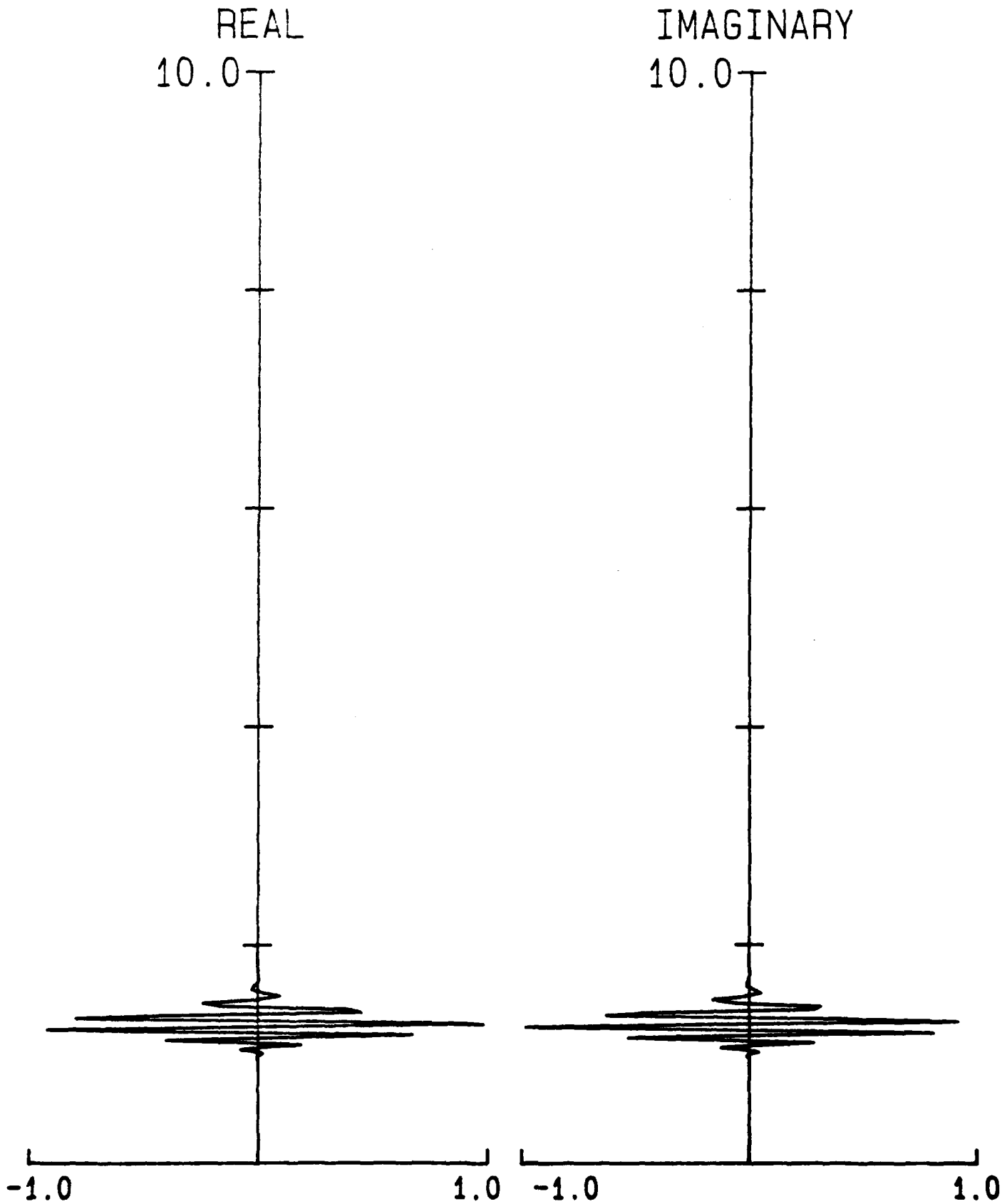

THE HOKENSON COMPANY

Fig. C8

TXY STRESS PERTUBATION

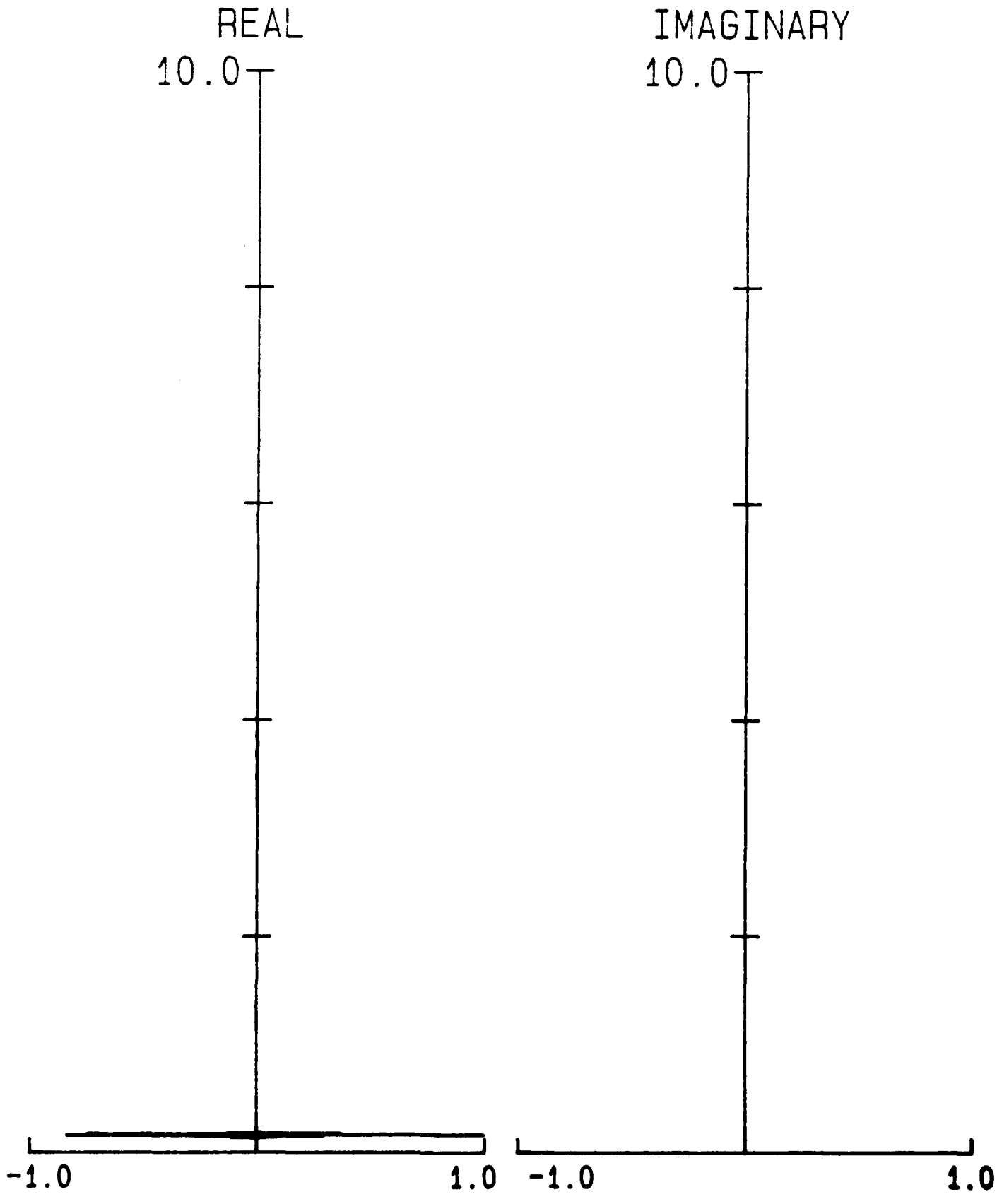

THE HOKENSON COMPANY

Fig. C9

TYY STRESS PERTUBATION

THE HOKENSON COMPANY

Fig. C10

TYZ STRESS PERTUBATION

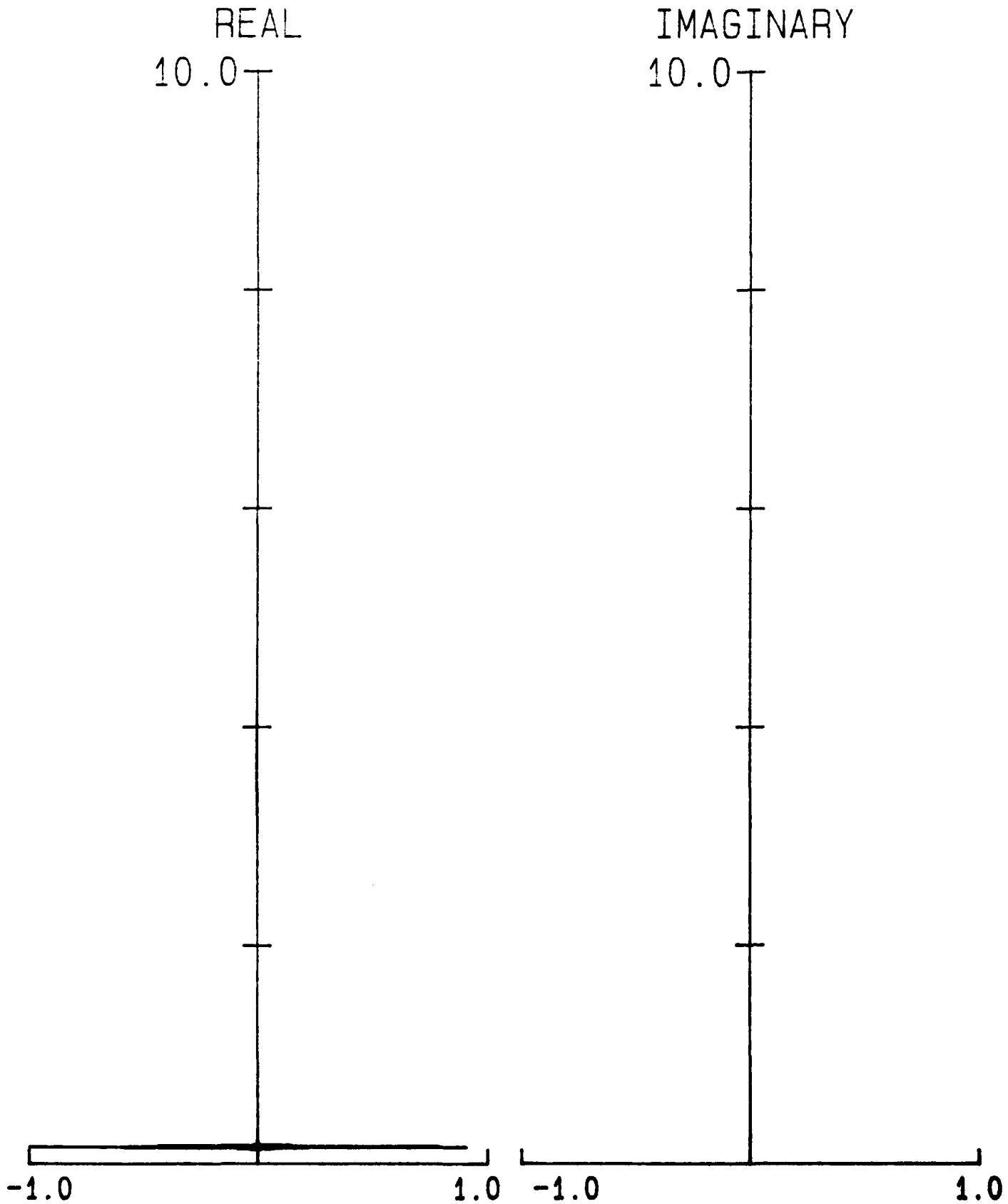

Figs. & Tables C11 - C13. Alpha Solutions For The Particular Cases Shown With Conditions Identical to Fig. C3 Except τ_ε is Non-Zero.

THE HOKENSON COMPANY

Fig. C11

BETA 0.100
OMEGA 2.000
EPSMAG 1.000
TAUEPS 1.000
RE NO. 44369.

SOLUTIONS OF ALPHA

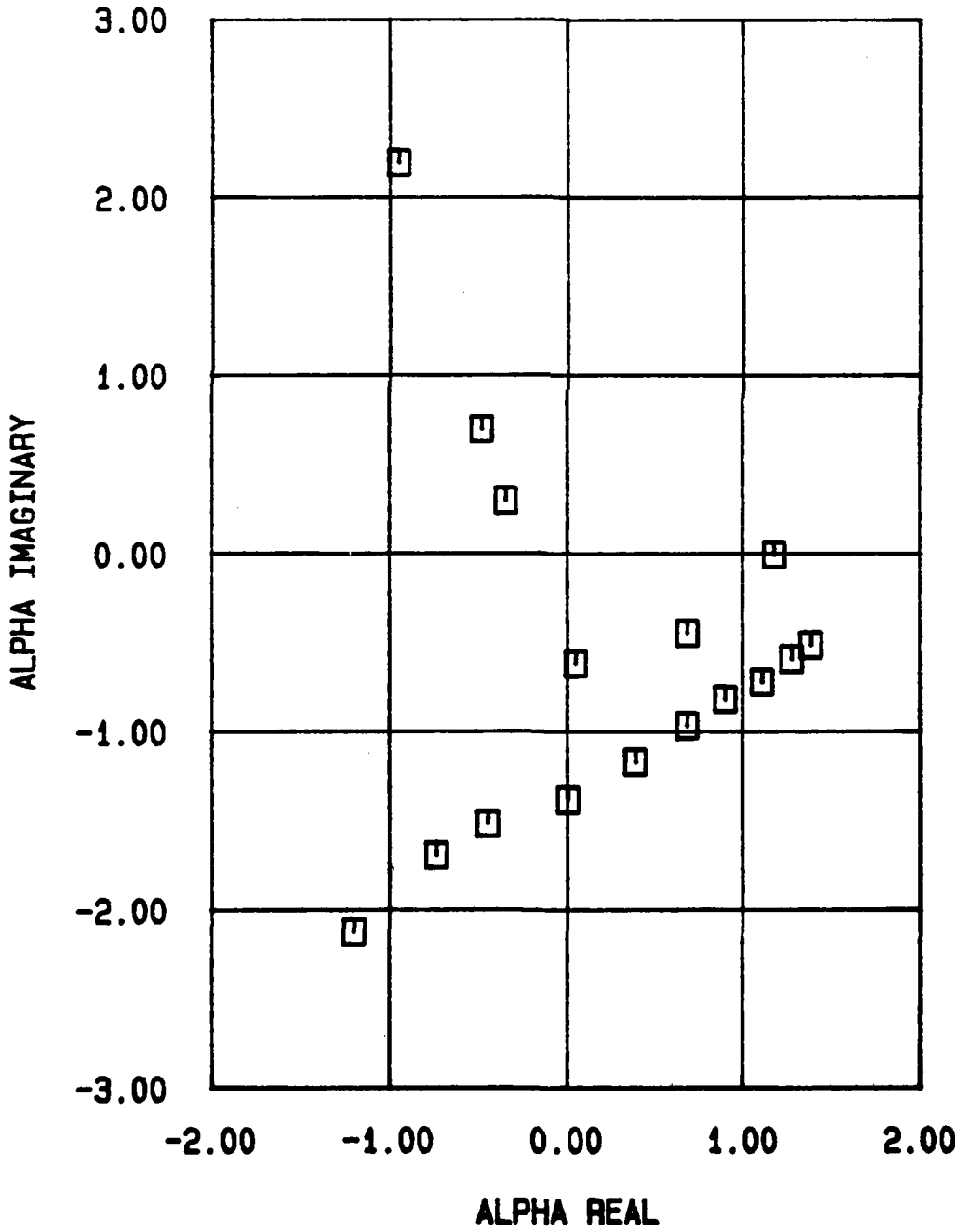

THE HOKENSON COMPANY

Table C11

BETA	0.100
OMEGA	2.000
EPSMAG	1.000
TAUEPS	1.000
RE NO.	44369.000

ALPHA REAL	ALPHA IMAGINARY	K	PHASE SPEED
0.04822	-0.61343	-12.72114	41.47530
-0.73597	-1.69037	2.29679	-2.71749
-1.19810	-2.12207	1.77120	-1.66932
0.38616	-1.16745	-3.02318	5.17913
0.00584	-1.38015	-236.44127	342.63199
-0.44789	-1.51448	3.38136	-4.46537
0.68070	-0.96358	-1.41556	2.93813
0.68239	-0.44285	-0.64897	2.93086
0.90013	-0.81632	-0.90690	2.22190
1.11133	-0.71862	-0.64663	1.79965
1.18127	-0.00043	-0.00036	1.69310
1.27817	-0.59046	-0.46196	1.56473
1.38630	-0.50984	-0.36777	1.44268
-0.34523	0.30375	-0.87984	-5.79327
-0.48100	0.70200	-1.45946	-4.15800
-0.95000	2.20000	-2.31579	-2.10526

THE HOKENSON COMPANY

Fig. C12

BETA 0.100
OMEGA 2.000
EPSMAG 1.000
TAUEPS 10.000
RE NO. 44369.

SOLUTIONS OF ALPHA

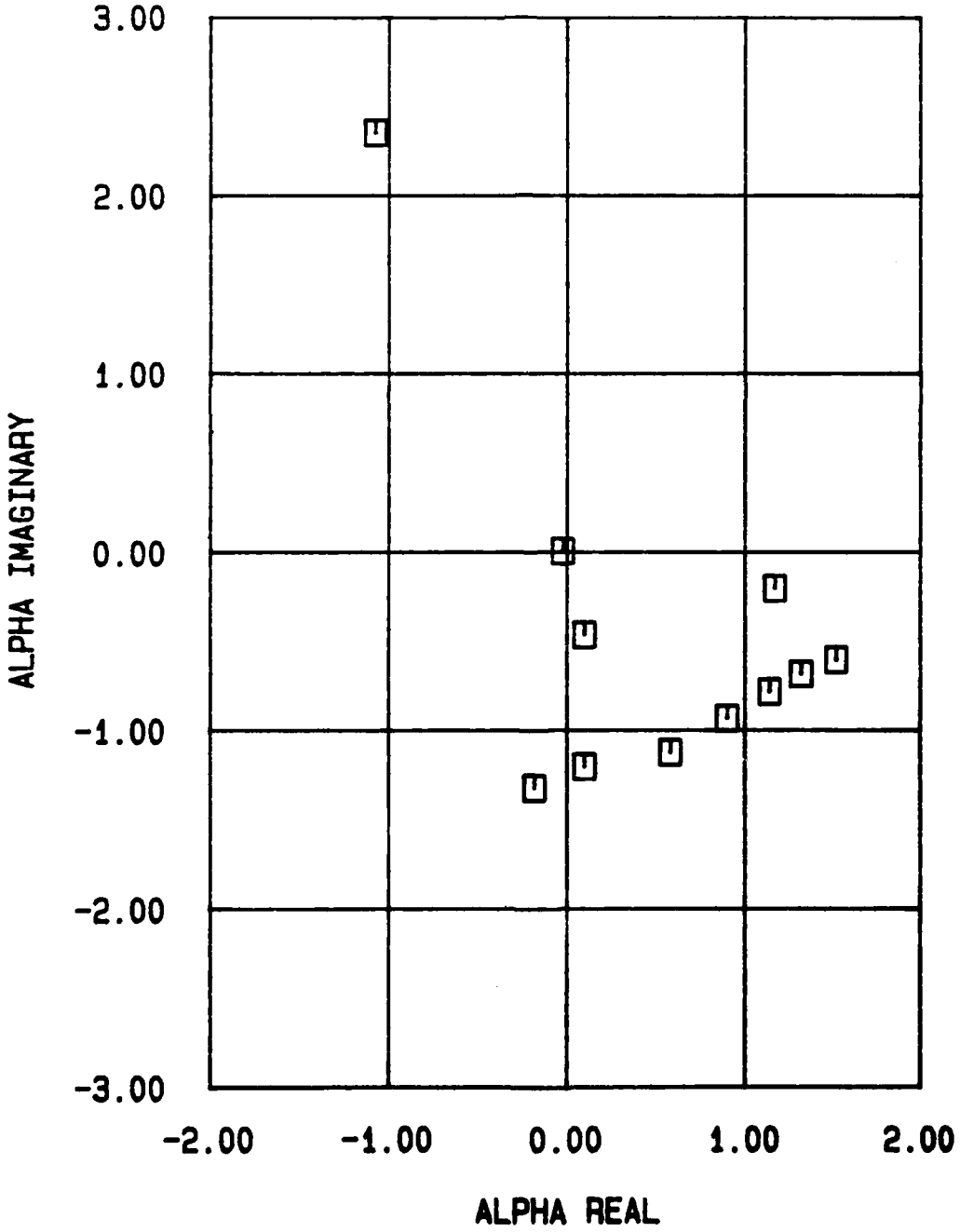

THE HOKENSON COMPANY

Table C12

BETA	0.100
OMEGA	2.000
EPSMAG	1.000
TAUEPS	10.000
RE NO.	44369.000

ALPHA REAL	ALPHA IMAGINARY	K	PHASE SPEED
0.10000	-0.46000	-4.60000	20.00000
-0.18000	-1.32000	7.33333	-11.11111
0.10000	-1.20000	-12.00000	20.00000
0.58000	-1.12000	-1.93103	3.44828
0.90000	-0.93000	-1.03333	2.22222
1.14000	-0.78000	-0.68421	1.75439
1.32000	-0.68000	-0.51515	1.51515
1.52000	-0.60000	-0.39474	1.31579
1.17000	-0.20000	-0.17094	1.70940
-1.07429	2.35657	-2.19360	-1.86169
-0.02175	0.00801	-0.36826	-91.94980

THE HOKENSON COMPANY

Fig. C13

BETA 0.100
OMEGA 2.000
EPSMAG 1.000
TAUEPS 30.000
RE NO. 44369.

SOLUTIONS OF ALPHA

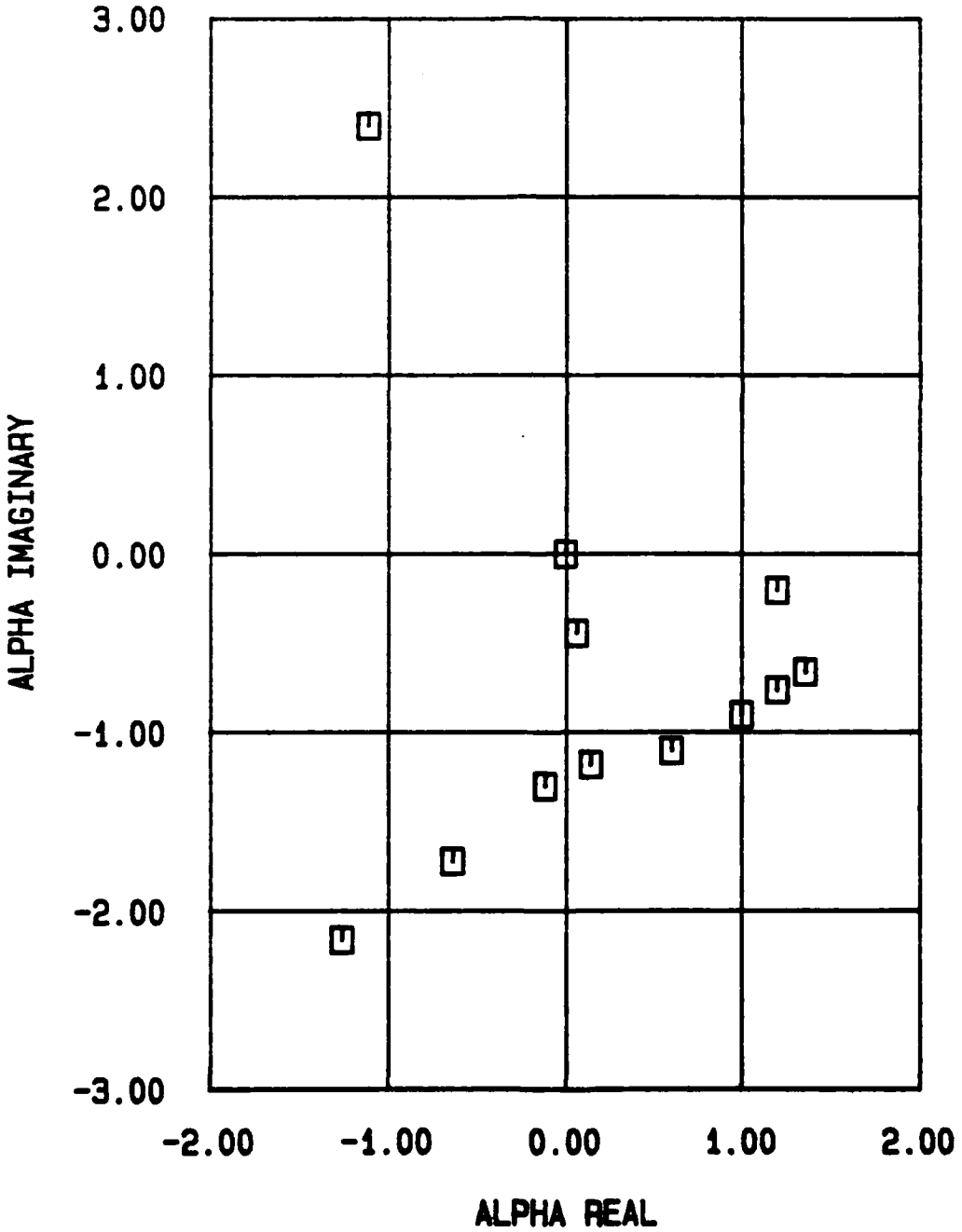

THE HOKENSON COMPANY

Table C13

BETA	0.100
OMEGA	2.000
EPSMAG	1.000
TAUEPS	30.000
RE NO.	44369.000

ALPHA REAL	ALPHA IMAGINARY	K	PHASE SPEED
0.06000	-0.44000	-7.33333	33.33334
-0.64000	-1.72000	2.68750	-3.12500
-1.26000	-2.16000	1.71429	-1.58730
0.60000	-1.10000	-1.83333	3.33333
1.00000	-0.90000	-0.90000	2.00000
1.20000	-0.76000	-0.63333	1.66667
1.20000	-0.20000	-0.16667	1.66667
1.36000	-0.66000	-0.48529	1.47059
0.14000	-1.18000	-8.42857	14.28571
-0.12000	-1.30000	10.83333	-16.66667
-1.11325	2.40235	-2.15796	-1.79654
-0.00350	-0.00050	0.14286	-571.42853

Figs. C14 a & b and Table C14. A Modified Input Eddy Viscosity Profile With The Peak Located Twice As Far From The Wall As In Previous Solutions. Alpha Solutions For The Particular Case Shown.

THE HOKENSON COMPANY

Fig. C14a

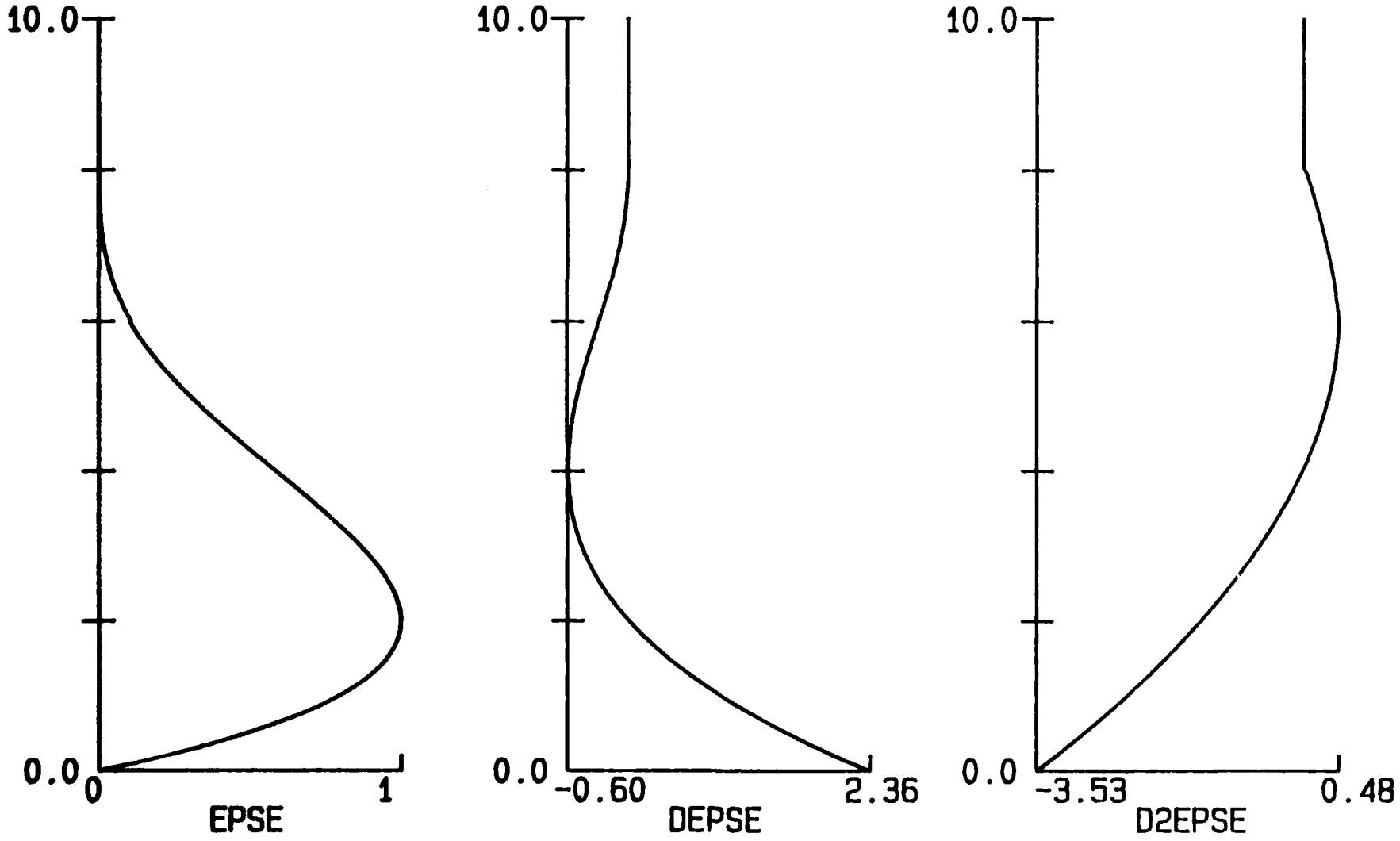

THE HOKENSON COMPANY

Fig. C14b

BETA 0.100
OMEGA 2.000
EPSMAG 1.000
TAUEPS 1.000
RE NO. 44369.

SOLUTIONS OF ALPHA

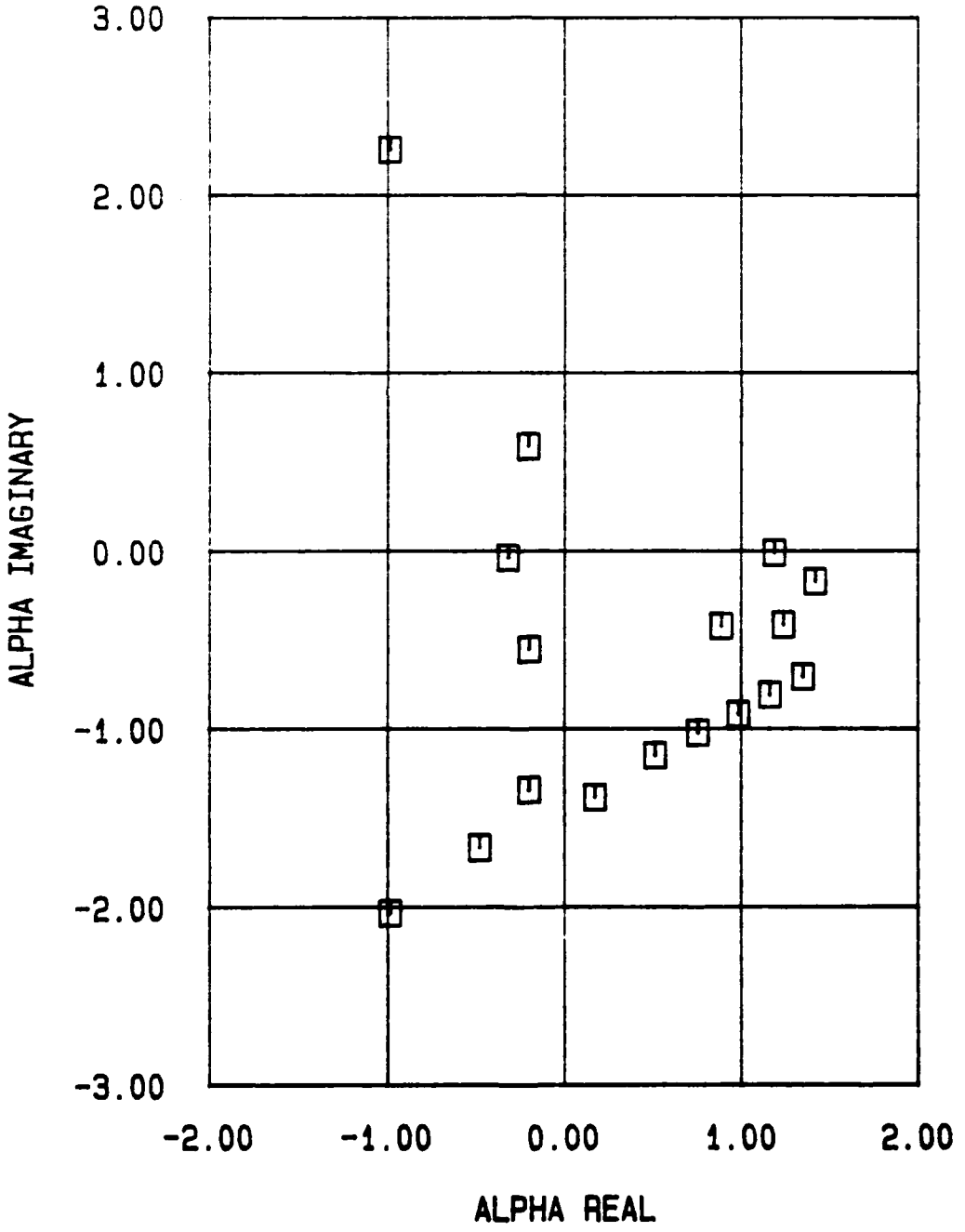

THE HOKENSON COMPANY

Table C14

BETA	0.100
OMEGA	2.000
EPSMAG	1.000
TAUEPS	1.000
RE NO.	44369.000

ALPHA REAL	ALPHA IMAGINARY	K	PHASE SPEED
-0.98400	-2.02950	2.06250	-2.03252
-0.48000	-1.66000	3.45833	-4.16667
-0.19800	-1.33600	6.74747	-10.10101
-0.19800	-0.54600	2.75758	-10.10101
0.17400	-1.38000	-7.93103	11.49425
0.51500	-1.14427	-2.22187	3.88350
0.75600	-1.01800	-1.34656	2.64550
0.98400	-0.91450	-0.92937	2.03252
1.16250	-0.80500	-0.69247	1.72043
1.34830	-0.70360	-0.52184	1.48335
0.88800	-0.41640	-0.46892	2.25225
1.23800	-0.40960	-0.33086	1.61551
1.41900	-0.16600	-0.11698	1.40944
1.18700	-0.00400	-0.00337	1.68492
-0.31800	-0.03200	0.10063	-6.28931
-0.20234	0.59344	-2.93289	-9.88435
-0.98600	2.26225	-2.29437	-2.02840

END
DATE
FILMD
3-88
DTIC